Investigation of Metal-Doped TiO_2 and Fenton-Like Reactions for Waste Water Decontamination

Howard Leroy Willett III

Advisor: Michael Hambourger, Ph.D.

Honors Thesis

Appalachian State University

A.R. Smith Department of Chemistry

525 Rivers Street, Boone, NC 28608

Submitted to the A. R. Smith Department of Chemistry

and The Honors College

in partial fulfillment of the requirements for the

University Honors and Chemistry Departmental Honors

July 2016

Approved by:

Michael Hambourger, Ph.D., Thesis Director,

_____

George Ehrdardt, Ph.D., Second Reader

_____

Dale E. Wheeler, Ph.D., Third Reader

_____

Libby Puckett, Ph.D., Departmental Honors Director

_____

Claudia Cartaya-Marin, Ph.D., Chemistry Departmental Chair

_____

Ted Zerucha, Ph.D., Interim Director, The Honors College

_____

Table of Contents

List of Figures

List of Abbreviations

4NA	N,N-dimethyl-*p*-nitrosoaniline
AR	Allura Red
AOP	advanced oxidation processes
CB	conductance band
COD	chemical oxygen demand
ECs	emerging contaminants
eV	electronvolt
FTO	fluorine-doped tin oxide
IIM	insoluble inorganic matter
IOM	insoluble organic matter
ITO	indium-doped tin oxide
PEG	polyethylene glycol
PEO	polyethylene oxide
PMS	peroxymonosulfate
ROS	reactive oxygen species
SIM	soluble inorganic matter
SOM	soluble organic matter
TNT	2,4,6-trinitrotoluene
TOC	total organic carbon
VB	valence band

Abstract

Access to clean drinking water is one of the most important problems our society faces in the coming future. In attempt to address this pervasive problem, advanced oxidation processes, such as derivatives of the Fenton reaction and iron-doped TiO_2, have been investigated as a means to purify water. Through monitoring Allura Red's (AR) absorbance, it was found that two common versions of the Fenton reaction, the Fe^{2+}/H_2O_2 and Co^{2+}/PMS (peroxymonosulfate) systems, have similar decolorization rates. Iron-doping TiO_2 is showing the desired lowering of the conduction band and band gap, but initial dye decolorization experiments are showing little decolorization of dye. Further testing with both methods must be investigated to develop a purification system capable of removing all water pollutants.

I. Introduction

Need for Clean Water

With an ever-growing population, clean water is quickly becoming scarce. An estimated 750 million people lack access to clean drinking water, about one of every nine people on Earth.[1] This problem is pervasive throughout the world; while a country may not lack access to water, it may consume water quicker than natural processes replace it, leading to a water deficit. This water scarcity fluctuates with seasonal consumption and weather.[2] Figure 1 illustrates the global distribution of this water deficit. Areas such as Mexico, Saharan Africa, and Australia are experiencing water scarcity almost 12 months per year, while many populated areas such as West Coast America, India, and China experience the

same water issue part of the year.

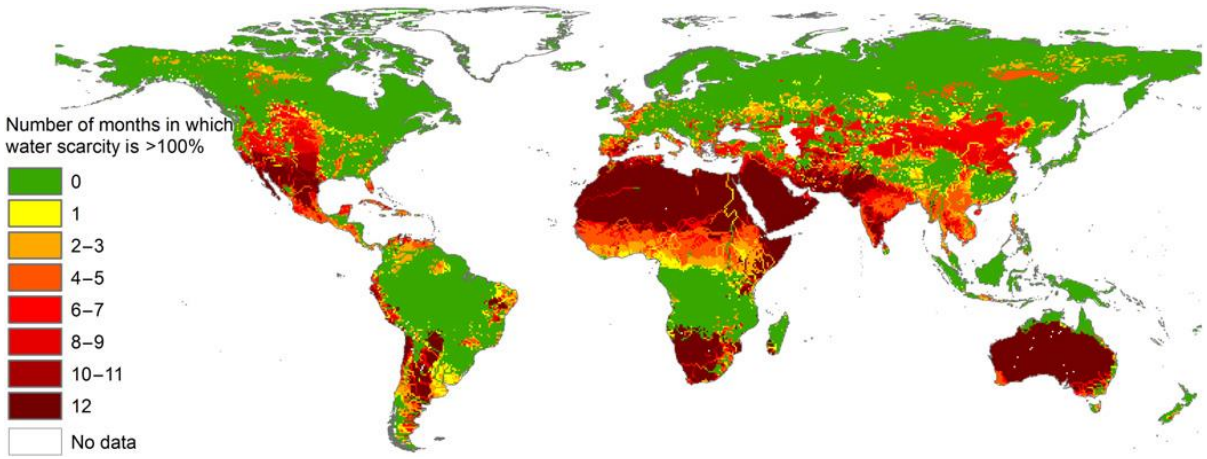

Figure 1. Water scarcity map. This figure shows the number of months an area runs a water deficit. The water deficit is defined as a month where the water taken from the environment exceeds the water replaced by natural processes such as rainfall. Figure adapted from reference 2.

One way to free up more available water is to purify waste water allowing its reuse. In developing countries, people continue to die at alarming rates due to diseases associated with improper water sanitation. Improper purification leads to water contamination which has been shown to cause an increase in the viral and bacterial load leading to a rise in morbidity and mortality of those drinking it.[3] While methods to purify water of these biological contaminants have been created and are in widespread use, fewer methods exist to reliably treat water for xenobiotic compounds. Antibiotics and other medicines, prescribed and not, occur in detectable quantities in ground water in the United States.[4] These drugs and their biological metabolites are not readily degraded in traditional waste water purification like biological contaminants, leading to a marked increase in the presence in surface waters as their usage continues.[5]

Detecting and identifying emerging contaminants (ECs) is another issue. Emerging contaminants are chemicals that are newly becoming widespread pollutants due to a wide variety of reasons including development of new products. While many ECs have been

identified, many are still being discovered and even more are created as new manufacturing processes are developed. With most technological advances, new sources of pollution come about, whether novel chemicals or an increase in the usage of a known chemical. Complicating this issue is a lack of government-established thresholds constituting permissible and impermissible levels for ECs.[6] Not only must these contaminants be identified, but their sources must be too. Many contaminants come from multiple sources, making identification of the pollutant even harder (Figure 2). Further investigations into how toxins accumulate in our environment may help to address the problem at the source and lower overall pollution.

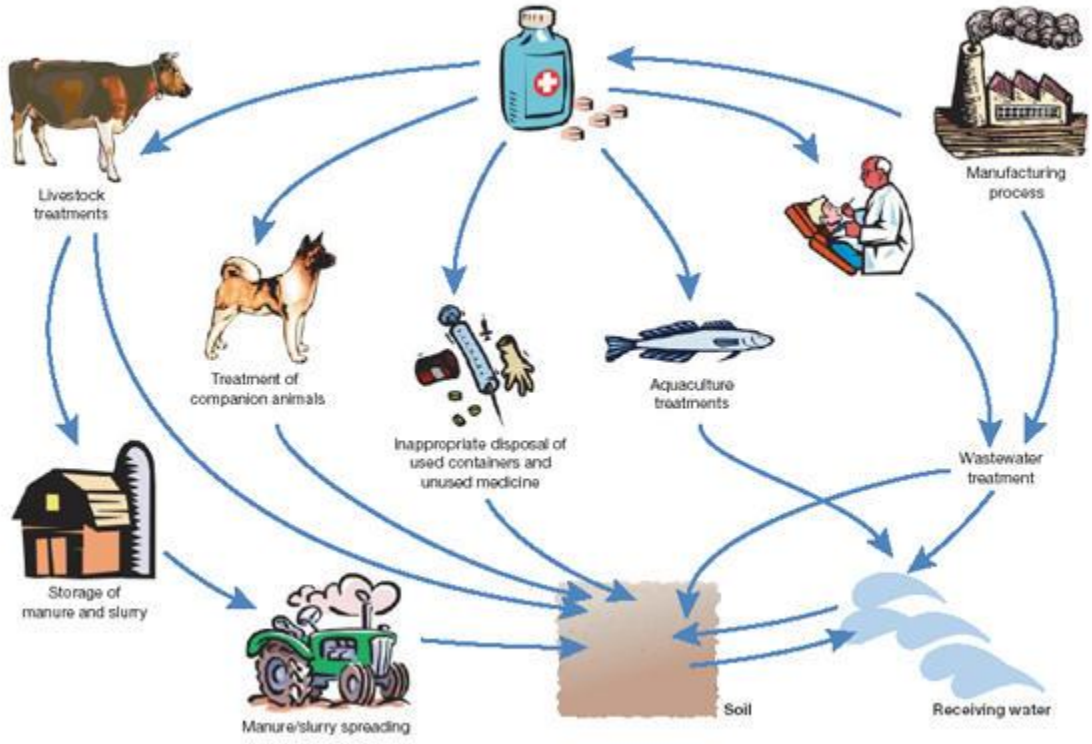

Figure 2. Medical contaminant cycle. This figure shows common routes for medical contaminants to enter the environment. Both animals and humans pass small amounts of medicine through their urine. Not all medical waste is filtered out at waste water treatment plants, leading to accumulation in the environment. Figure adapted from reference 7.

Another issue associated with ECs is the uncertainty in their natural degradation pathways and associated timelines. While many contaminants may breakdown into harmless products, many do not, and in fact, increase their toxicity as they breakdown. Soil contaminated with TNT, 2,4,6-trinitrotoluene, increases in toxicity to *Enchytraeus crypticus*, a soil worm commonly used to as a model species for soil toxicology.[8] When a contaminant is known, it is easy to test its toxicity and the toxicity of its natural degradation products, but with the number of ECs growing, they are not all known and neither are all the natural degradation pathways.

Many of the identified ECs are in concentrations high enough to cause environmental damage or induce effects in wildlife.[7] Compounds capable of inducing sex changes in fish, amphibians, and reptiles have been found in biologically relevant levels in multiple water systems.[9] Many organisms in their prenatal or young stages are sensitive to endocrine disruptors, which have permanent effects on growth and development. ECs have been linked to a decline in fish populations.[9] For example, perchlorate has been detected and found widely present in ground and surface waters as well as wild plant and animal species.[10] Perchlorate acts as an endocrine disruptor inducing reproductive mutations and sexual changes in amphibian and reptile species.[10] As an inorganic contaminant, perchlorate will not be purified in the same manner as organic contaminants, but causes similar problems. While immediate effects of some pollutants are known, it is complicated to completely understand the scope of their effects. For example, antibacterial chemicals leeched into the soil may kill microbes responsible for breaking down pesticides, leading to an increase in the pesticide levels of water, affecting other species.[7]

Traditional Water Purification

Traditional methods of waste water purification typically involve two steps: a primary and secondary treatment (Figure 3). Waste water is filtered to remove insoluble inorganic matter (IIM) and particulate waste. The remaining effluent is put into a holding tank to settle, allowing insoluble organic matter (IOM) to settle into a sludge.[11] The underflow containing the primary sludge and IOM is removed for treatment and the overflow containing the waste water is removed for secondary biochemical treatment. This biochemical treatment process varies at the plant where the water is treated, but all processes rely on a mixture of microorganisms to breakdown soluble organic matter (SOM) and soluble inorganic matter (SIM).[11] Much of the organic matter is tied up in the biomass of the microorganisms. The underflow containing the microorganism biomass and residual IOM is removed forming the secondary sludge.

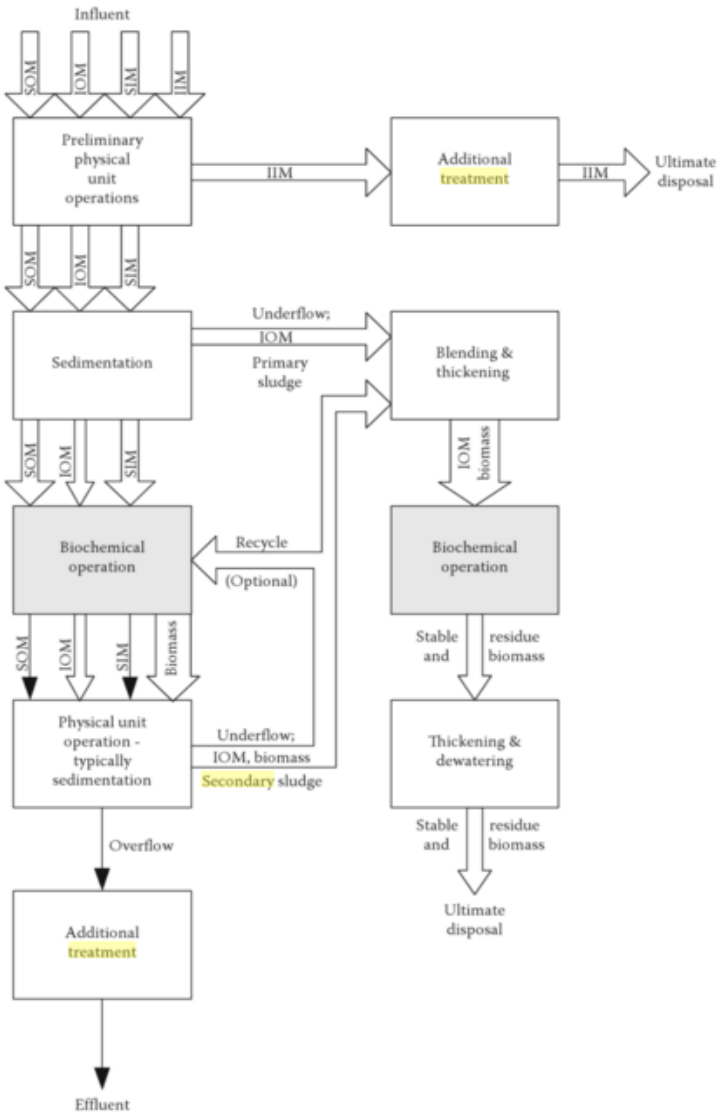

Figure 3. Traditional waste water purification. Traditional waste water purification implemented in the United States includes a primary treatment and secondary treatment step. Figure reproduced from reference 11.

Both primary and secondary sludge are generally concentrated and treated together. The treated water from the secondary step may be further treated depending on the plant and what contaminants remain, but in most cases no further steps are required by law prior to the release of treated water into the environment.[11] This treatment method is great for insoluble materials and many soluble chemicals, but is not effective at removing all compounds.

Beta-blockers and psycho-active drugs have been shown to be degraded with less than sixty percent efficacy.[12] SOM and SIM continue to be an issue for wide-scale removal. Two important characteristics used to monitor the quality of waste water are chemical oxygen demand (COD) and total organic carbon (TOC). COD is the amount of oxygen it would take to completely oxidize soluble and particulate organic matter, whereas TOC is a direct measurement of the organic carbon in solution.

Traditional methods for purification of these contaminants, while effective, are not cost effective and require too much investment and infrastructure to be useful in many settings.[13] Ozonolysis and reverse osmosis both require large amounts of energy, either in synthesis required chemicals or driving the process. Many contaminants also have an established protocol for removal, but requiring different decontamination methods for each contaminant is expensive and impractical.[7] In order to circumvent the need for a tailored procedure for each contaminant, one powerful reaction could be utilized. In an attempt to purify water of a wide scope of contaminants, strong oxidants have traditionally been employed to destroy compounds rather than filter them out. Powerful advanced oxidation processes (AOP) including the tradition Fenton reaction and derivatives, their photochemical equivalents, semiconductor mediated oxidation, and traditional chemical methods, are employed to purify waste water of varying chemical pollutants.

Fenton Chemistry

In most AOP, hydroxyl radicals are responsible for the chemical oxidation of waste water contaminants. These radicals are powerful oxidants, capable of breaking down almost all organic molecules. Hydroxyl radicals are also able to further react and create other reactive oxygen species (ROS). Hydroxyl radicals can be formed from various sources, but a

common route is through the reduction of molecular dioxygen (O_2), forming superoxide as an intermediate. Superoxide can further react in aqueous environments to produce ROS such as more hydroxyl radicals, hydrogen peroxide, or peroxyl radicals (Figure 4).[14]

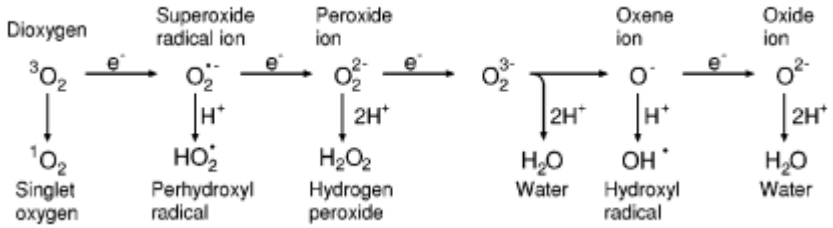

Figure 4. Reactive oxygen species interplay. Reduction of diatomic oxygen can result in the superoxide ion. This ion is capable of subsequent reactions to form peroxyl radicals (perhydroxyl), hydrogen peroxide, or hydroxyl radicals. Figure adapted from reference 14.

All of the formed ROS are unstable and capable of breaking down organic molecules. Many of these ROS are formed via oxidation of another compound. For example, superoxide is extremely oxidizing and can remove an electron from many organic molecules forming an organic radical species that will spontaneously decompose or further react in solution.[14] Many waste water purification techniques take advantages of the oxidizing strength of ROS in order to break down contaminants.

The Fenton reaction was first identified by Henry John Horstman Fenton as he noted the effects of the ferrous ion on tartic acid solutions in the presence of varying oxidants, most notably, hydrogen peroxide.[15] Fenton went on to publish the oxidation of various organic compounds including other organic acids and polyhydric alcohols.[16,17] Fenton detailed the oxidation processes at play and also documented increased catalytic oxidation in the presence of sunlight.[15] Based on the widely accepted mechanism of the Fenton reaction, ferrous iron catalyzes the decomposition of hydrogen peroxide leading to the production of hydroxyl radicals. These radicals are responsible for the oxidation of organic compounds. The Fenton

reaction plays an important role in the creation of radicals in the body and is essential for the bodies defense against foreign invaders.[18] These radicals and generated ROS play critical roles in cell signaling pathways including cell death.[19] Radical species created by the Fenton reaction have been linked to food spoilage and material aging.[20] The Fenton reaction and ROS are important in many fields of chemistry and biology.

While the reaction has been studied for over one hundred years, the exact mechanistic steps remain unknown. Currently, two different pathways are proposed: one that includes the formation of a radical immediate, and one that involves the formation of a ferryl ion. The general reaction labeled the 'Fenton reaction' is ferrous iron catalyzed decomposition of hydrogen peroxide leading to the production of hydroxyl radicals (*Reaction 1*).[21]

$$Fe^{2+} + H_2O_2 \rightarrow Fe^{3+} + OH^- + OH^{\bullet} \quad (1)$$

Hydroxyl radicals may react with water or organic pollutants, oxidizing the compound and producing more radicals. These radicals are then able to participate in a series of reactions leading to the further oxidation of organic compounds. In the absence of a pollutant, hydroxyl radicals are also able to react with peroxide to form peroxyl radicals. (*Reaction 2*).

$$OH^{\bullet} + H_2O_2 \rightarrow HO_2^{\bullet} + H_2O \quad (2)$$

Peroxyl and hydroxyl radicals can react with water or oxygen to form other reactive oxygen species (ROS). The peroxyl radical is able to react with ferric iron to regenerate the catalytic form of iron (*Reaction 3*).

$$Fe^{3+} + HO_2^{\bullet} \rightarrow Fe^{2+} + H^+ + O_2 \quad (3)$$

Radicals can also oxidize ferrous iron turning it into ferric iron, wasting a radical and the catalytic form of iron (*Reactions 4 and 5*).

$$Fe^{2+} + HO_2^{\bullet} \rightarrow Fe^{3+} + HO_2^{-} \quad (4)$$

$$Fe^{2+} + OH^{\bullet} \rightarrow Fe^{3+} + OH^{-} \quad (5)$$

In contrast to this long accepted series of reactions, recent calculations suggest that the ferryl ion may play a role in the oxidation of water contaminants.[22] Determining which pathway is responsible for the Fenton reaction's oxidative power is made even more complicated because both pathways likely compete kinetically. The initial step in both reactions involves hydrogen peroxide bonding with iron(II), followed by cleavage of the oxygen-oxygen bond in peroxide. Through free energy calculations, it was determined the reaction favors the formation of the ferryl iron oxide compound capable of oxidation.[22]

This lack of insight into the mechanism has not prevented the Fenton reaction from being used to purify waste water. The success of the Fenton reaction has led to the discovery of a whole subset of oxidation reactions labeled Fenton-like reactions. Different first-row transition metals have been shown to catalyze oxidation reactions in the presence of hydrogen peroxide.[23] These metals have their own chemical properties making the Fenton systems created with each different. Metals that participate in Fenton-like oxidation reactions are generally thought to proceed through the same radical pathway as iron in Reactions 1-5 (*Reactions 6-10*), although it is possible other pathways are involved.[21]

$$M^{n+} + H_2O_2 \rightarrow M^{n+1} + OH^- + OH^\bullet \quad (6)$$

$$OH^\bullet + H_2O_2 \rightarrow HO_2^\bullet + H_2O \quad (7)$$

$$M^{n+1} + HO_2^\bullet \rightarrow M^{n+} + H^+ + O_2 \quad (8)$$

$$M^{n+} + HO_2^\bullet \rightarrow M^{n+1} + HO_2^- \quad (9)$$

$$M^{n+} + OH^\bullet \rightarrow M^{n+1} + OH^- \quad (10)$$

Another factor to consider when utilizing Fenton chemistry is the Photo-Fenton reaction. The Fenton reaction has shown an increased rate of reaction in the presence of light due to the photoreduction of ferric into ferrous iron, generating more catalyst for the reaction. This photoreduction has been shown to increase the rates for Fenton-like reactions as well. For the Fenton reaction, involving ferrous iron and hydrogen peroxide, sunlight has been shown to increase the rate of reaction by as much as 3.9 times.[24] Overall, photo-assisted versions of Fenton-chemistry increase the rate of decrease in TOC, dye absorbance, and COD.[24]

Fenton reagents react in a homogenous manner; all of the components of the reaction are in the aqueous phase. For the Fenton reaction this poses two problems: the solubility of iron, requiring low pH, and the need for a catalyst separation step.[25] The Fenton reaction generates hydroxide ions, which increase the pH of the solution. This may form insoluble iron(III) hydroxide solid, removing active iron catalyst from solution. Precipitation of the iron catalyst can be prevented by keeping the pH under 2, but in order to remove iron catalyst after waste water purification, the pH of the solution is raised intentionally to form solid iron(III) hydroxide to be filtered out. The provided Pourbaix diagram shows the complex relationship of iron in an aqueous solution as a function of pH and redox potential (Figure 5).

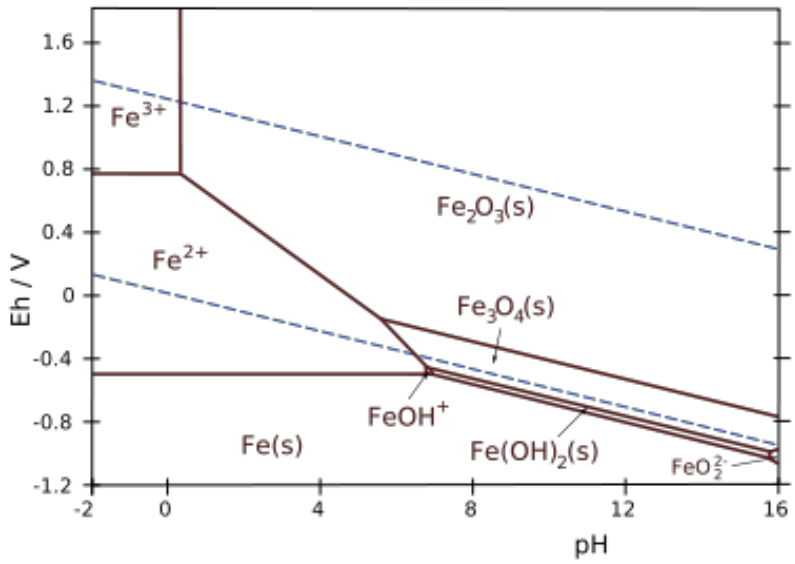

Figure 5. Pourbaix diagram of iron. Redox potential graphed versus pH of solution to show which iron compound exists. As shown, for catalytic iron to be present, the pH must be below ~3. $Fe(OH)_3$ is a solid that precipitates out of solution. This highlights an important limitation of using iron as a Fenton catalyst for waste water production. Figure adapted from reference 26.

This problem can be addressed by manipulating the catalyst into a heterogeneous catalyst in which the catalyst is not dissolved into solution. The metal catalyst can be immobilized in a zeolite, silica, clay, or activated carbon matrix.[27] Heterogeneous catalysts are complicated as they require special attention to active site structure as catalytic activity is limited to the interface between the solid iron species and solution. Through optimization, effective heterogeneous catalytic systems have been created and shown to catalyze degradation of model compounds.[27] These systems do not leech significant iron into solution allowing reuse of the catalyst without the need for purification of the water at the end. Herney-Ramirez et al. used clay to immobilize various iron salts in a solid matrix and monitored a 0.1M orange dye solution to determine the effectiveness in waste water purification using hydrogen peroxide as an oxidant.[28] After four hours, these systems showed around 65% TOC removal with little

iron leeching into solution.[28] These catalysts do show diminishing performance after each use, which may be due to iron slowly leeching out of the material.

In addition to changing the metal, the oxidant can also be changed in the Fenton reaction. Systems utilizing the Fenton-like decomposition of Oxone™ by Co^{2+} have shown great effectiveness in bleaching various dyes.[29] Oxone™ serves as a source of peroxymonosulfate ions (PMS). Oxone™ is a mixture of potassium peroxymonosulfate, potassium sulfate, and tetrabutylammonium to balance charge. The sulfate ions are present to offset the equilibrium of the disassociation of peroxymonosulfate and extend the shelf life of the compound.

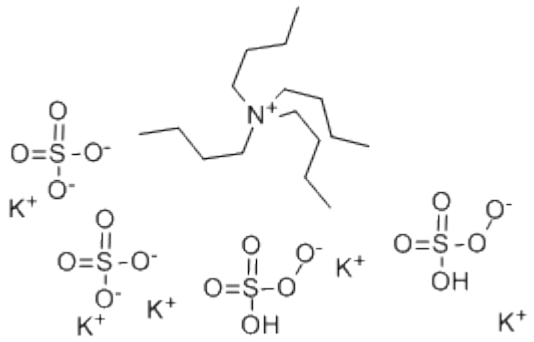

Figure 6. Oxone™. This figure shows what one 'molecule' of Oxone™ looks like. It is actually a collection of sulfate, peroxymonosulfate, potassium, and tetrabutylammonium ions, but the PMS ions serve as a source of sulfate radicals.

The catalyzed decomposition of PMS by cobalt(II) leads to a radical chain reaction that produces hydrogen sulfate and oxygen gas (*Equation 11*).[30]

$$2\ HOOSO_3^- \rightarrow O_2 + 2HSO_4^- \qquad (11)$$

The first two reactions of this breakdown produce sulfate radicals that are of interest for waste water purification (*Equations 12-13*).[30]

$$Co^{2+} + H_2O \leftrightarrow CoOH^+ + H^+ \qquad (12)$$

$$CoOH^+ + HOOSO_3^- \rightarrow CoO^+ + H_2O + SO_4^{\bullet -} \qquad (13)$$

These radicals can react with organic pollutants just like hydroxyl radicals. Oxone™, a common source of sulfate radicals, costs 3-3.5 times as much as hydrogen peroxide (prices based upon Sigma-Aldrich June, 2016). Sulfate radicals may be used to produce an effective waste water purification method, but the improvement to the system must outweigh the increased cost it takes to produce over hydrogen peroxide.

Semiconductor-mediated Waste Water Treatment

Another effective way to purify waste water involves oxidation by a semiconductor. Many semiconductors, TiO_2 included, are colloidal suspensions of small, solid particles in solution. These particles will settle out of solutions, requiring no filtration. Some are stirred as a solid powder while others are made into solid sheets. Oxidation via semiconductor also does not require the addition of an oxidant such as H_2O_2 or Oxone™ like the Fenton reaction does. Semiconductors exhibit a wide range of properties of industrial significance, but for waste water purification the light-sensitive properties are extremely important.[31] Properties including conductivity and band gap energy of the semiconductor must then be chosen to fit waste water purification.

Upon absorption of light, semiconductors form an 'electron-hole pair' (Figure 7). Semiconductor compounds lack empty electron orbitals close in energy to the valence band (VB) electrons. An excited electronic state is formed when a valence band electron is promoted to the conduction band (CB) via excitation by light or electricity of appropriate energy. The difference in energy of these two states is referred to as the band gap energy (E_g). [32] The excited state generally is stable on the nanosecond timescale, in which recombination or transfer of the formed charged states occurs. From the excited state, the positive hole is able to oxidize both pollutants and water. Oxidizing water leads to the

formation of hydroxyl radicals and other ROS. The conduction band electron is then free to reduce oxygen to superoxide which is also able to create more ROS. Both separated charges participate in breaking down pollutants in solution.

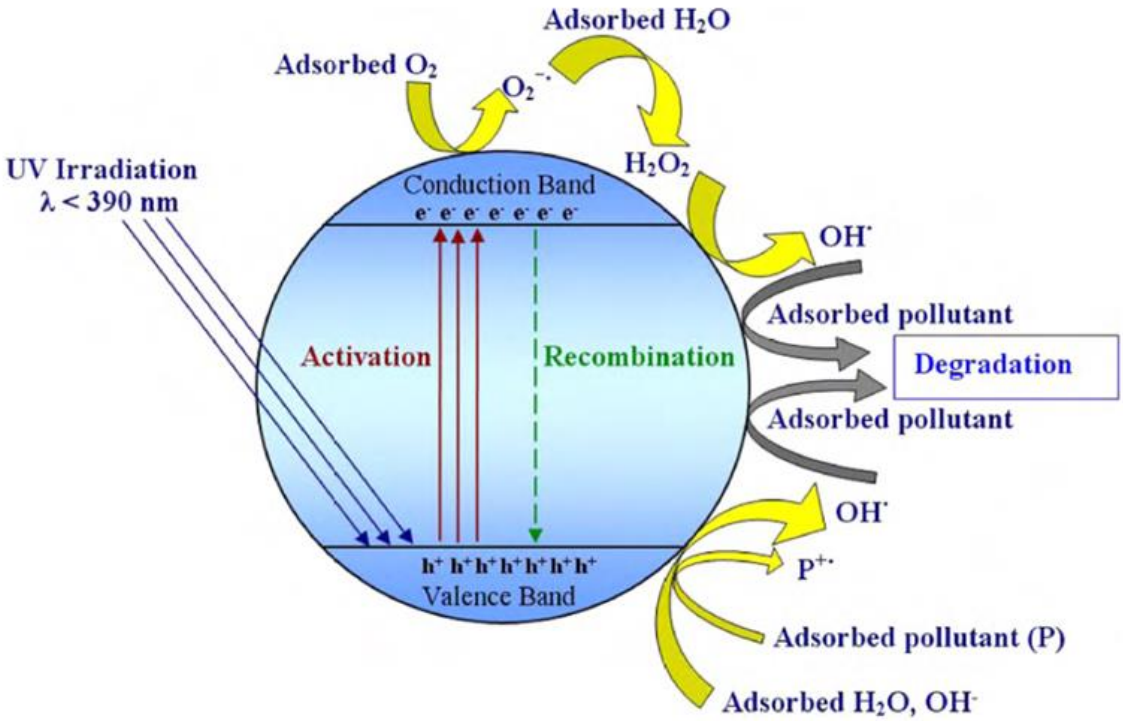

Figure 7. Semiconductor electron promotion schematic. This is the catalytic schematic for oxidation and reduction by the conduction band electron and valence band hole. Specific reactions depend upon what is adhered to the surface of the TiO_2 matrix and close by to react. UV radiation is needed for promotion of the valence band electron. Figure adapted from source 33.

One issue associated with semiconductor purification is the recombination of the positive hole and negative electron releasing energy as heat.[32] Imperfections in the crystal lattice of a semiconductor may slow the recombination of the charges following band gap excitation. Imperfections can include differences in oxidation state or the existence of different compounds. TiO_2, titanium(IV) oxide, for example, traps photo-generated electrons to form reduced Ti^{3+} sites, often located near the surface of TiO_2 particles. The addition of small amounts of certain transition metals such as Fe^{3+} and Cu^{2+} have been shown to prevent

recombination of electron-hole pairs.[32] While small amounts of these metals have shown to increase the effectiveness of TiO_2, too high of a concentration has a detrimental effect on its catalytic activity. Other transition metals like Cr^{3+} have increased the rate of recombination, decreasing the effectiveness of TiO_2 as a photocatalyst.[32]

The positively charged hole oxidizes compounds in physical contact with the semiconductor surface. If pollutant molecules are not in contact with the surface, semiconductors are capable of oxidizing water to form powerful hydroxyl radicals that are also capable of oxidizing molecules in solution.[32] In addition to the oxidation by the valence-band hole, the conduction band electrons are capable of reducing a variety of compounds. Conduction band electrons reduce a variety of inorganic compounds such as oxygen.[32] For reactions in aqueous solutions, the reduction of oxygen into superoxide is important. Oxygen acts as an electron scavenger, preventing recombination of the electron-hole pair improving the quantum yield of productive oxidants.[34] As previously stated, the superoxide radical also participates in the formation of other ROS.

In order to create a cost-effective waste water treatment process, TiO_2 is commonly used as it is cheap and stable in water under irradiation. TiO_2 has shown to be stable and photo-catalytically active as a n-type semiconductor that produces extremely powerful oxidizing valence band holes.[35] Both crystalline structures of TiO_2, rutile and anatase, are photo-catalytically active, with anatase having a higher rate of reaction. Anatase TiO_2 has a rather large band gap of 3.1 eV.[32] This band gap means TiO_2 requires near UV-light of less than 415 nm to promote photocatalysis.[35] Systems using TiO_2 as a catalyst require a constant supply of UV light or electricity to work, making them too expensive for general use as this light is not in high quantities in sunlight[36] (Figure 8). Transition metal doping has been

shown to increase the catalytic rate of TiO_2 at longer wavelengths.[37] Experiments have shown that in addition to preventing recombination of charged states, dopants may also play a role in accepting light that can promote electrons in the semiconductor.[37] Iron especially has been shown to absorb light and conduct the absorbed energy into the TiO_2 matrix allowing for band-gap promotion of electrons.

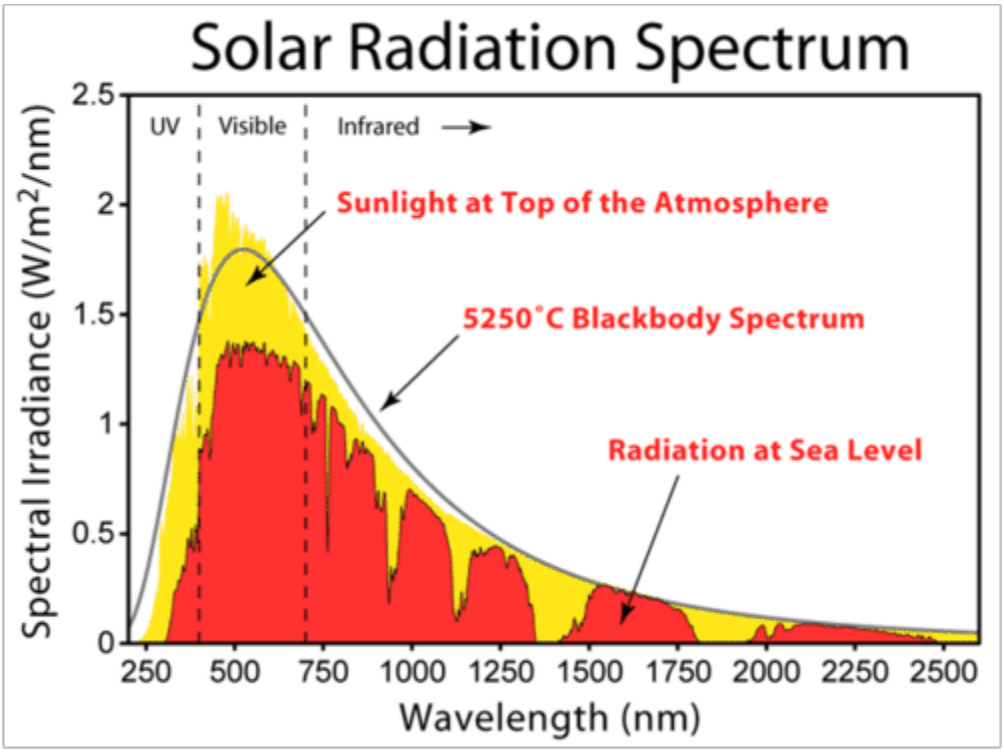

Figure 8. Sunlight wavelength distribution. As shown by the graph, solar light consists primarily of visible and near-infrared light. A semiconductor required UV light, such as TiO_2 would not be efficiently powered by sunlight alone and would require and external energy source. Figure adapted from reference 38.

Dr. Hambourger's research lab has previously investigated copper-doped TiO_2 which shows a decreased band gap in response to increased copper incorporation into the crystalline matrix of TiO_2. Initial data shows a similar effect with iron-doped TiO_2. Studies have shown that systems which utilize doped TiO_2 react in a colloidal, heterogeneous manner and have been effective at purifying waste water.[39] Studies have also shown TiO_2 capable of oxidizing organic compounds and using the electrons to reduce protons into hydrogen gas.[40] The lab

would like to utilize TiO_2 to develop an effective photocatalyst capable of converting organic pollutants into hydrogen fuel and nontoxic gases such as carbon dioxide and oxygen.

Project Outlook

Both the Fenton reaction and TiO_2 have been investigated and utilized for waste water treatment. The Fenton reaction has been implemented as a way to treat industrial waste water for specific contaminants that are not easily removed under traditional treatment, such as xylidine.[41] TiO_2 has also been investigated for its ability to oxidize organic and inorganic pollutants in water to purify waste water.[42] Our lab aims to produce a waste water purification method capable of purifying a wide array of compounds under various conditions, including recalcitrant pollutants not removed by current methods required in the United States, by means of monitoring dye decolorization of various Fenton-like systems and doped-TiO_2.

Initially the project was to investigate the ability to shift the band gap of iron-doped TiO_2 in hopes of developing a working waste water treatment method driven by visible light. After a semester of work, plans were made to collaborate with Dr. Erick Bandala at the Universidad de las Américas Puebla in San Andrés Cholula, Pue., Mexico. I was to use Dr. Bandala's total organic carbon analyzer for my iron-doped TiO_2 project, but due to unforeseen circumstances, I was asked to work on Fenton chemistry for waste water purification. I was tasked with comparing the Co^{2+}/ Oxone™ and traditional Fe^{2+}/H_2O_2 Fenton systems. Upon returning to Appalachian, I took this a step further and analyzed more metals: cobalt, nickel, iron, and manganese with both oxidants hydrogen peroxide and Oxone™. Goals for the projected included identifying metals capable of dye decolorization

and comparing the different oxidants on this decolorization while attempting to verify conclusions made in Mexico.

II. Experimental

Reagents

Anhydrous ferrous sulfate was purchased from J. T. Baker (Central Valley, PA). All other chemicals, unless otherwise stated, were purchased from Sigma-Aldrich (St. Louis, MO). All reagents were used as received unless otherwise stated. Deionized water obtained from department faucets was used in all experiments. Water used in bulk electrolysis experimentation was degassed under a nitrogen environment.

Instrumentation

UV-visible spectra and kinetic traces were obtained with a 1-cm path length quartz cuvette using a Shimadzu UV 2401 or Shimadzu UV-2600 spectrophotometer. Some kinetic experiments obtaining individual time point data were conducted with a Vernier LabQuest handheld using the Vernier SpectroVis Plus spectrophotometer + fluorometer. A WaveNow Potentiostat from Pine Instruments (Grove City, PA) and a Coy Labs glovebox with a palladium catalyst kept under 4% H_2 and 96% N_2 environment were used for bulk electrolysis measurements. An analytical balance was used.

TiO_2 Synthesis

Titanium(IV) oxide was synthesized using modifications of the method published by Kang *et al.*[43] Under a N_2 environment, a flask was charged with 8.9 mL of glacial acetic acid, 25 mL of H_2O, any desired iron precursor, and stirred on ice. Another flask was prepared under N_2 with 6.0 mL of isopropanol and 4.2 mL of titanium(IV) isopropoxide. The solution containing the titanium(IV) isopropoxide was added drop-wise via cannula addition or

syringe transfer to the acetic acid solution flask at a drop per second rate and refluxed. Of the resulting solution, 37 mL was loaded in a Parr digestion bomb (Parr Instrument Company, Moline, IL: Model 4744 General Purpose, 45 mL volume) and heated at 200 ºC for 12-16 hours. The resulting solution was sonicated for 30 minutes and then the solvent was removed under reduced pressure resulting in a viscous paste to which 20 wt% polyethylene oxide (PEO) and 20 wt% polyethylene glycol (PEG) were added (wt% in regards to final solid mass) as a binding agent. The resulting paste was stored under anaerobic conditions.

The TiO_2 pastes were spread onto 3 mm-wide ITO plates (Delta Technologies, LTD, Loveland, CO) and 10 mm-wide FTO plates (Hartford Glass Company, Hartford, IN) for further testing and characterization. Squares were made on the plates by taping strips of glass to bar them off. The paste was then spread across the plate. The plate was heated at 400 ºC for 30 minutes, burning off the PEG and PEO leaving the doped or undoped TiO_2 attached to the conductive glass.

Procedures

Conduction Band Determination

In order to test for the presence of conduction band electrons, TiO_2 was prepared on indium-doped tin oxide (ITO; Delta Technologies CB-50IN-CUV) plates rather than FTO. Varying potentials were applied to the TiO_2 -ITO electric plates. The ITO plates were connected to a potentiostat and submerged in a 1 mm pathlength UV-visible cuvette in deoxygenated water in the anaerobic glovebox. A platinum wire counter electrode and Ag/AgCl (3 M KCl) reference were used. The absorbance at 780 nm of the TiO_2 was monitored via UV-visible as varying negative potentials were applied to the plate. Potentials starting at -0.1 to -1.0 V were applied for one minute or until absorbance was stabilized and

then the next potential was applied. This was repeated for plates of varying iron concentration. Procedure adapted from Redmond *et al.*[44]

Band Gap Energy (E_g) Determination

To determine the band gap energy, absorbance of the solid TiO_2 semiconductors was taken. A linear fit was applied to the linear portion of the exponential rise, typically between 300-400 nm, and the intersection of the line and the x-axis for 0 absorbance was taken to be E_g. This value must be converted from wavelength of light, to the energy of light at that wavelength, to electron volts (eV). This can be done because the semiconductor will accept light with enough energy to promote electrons from the VB to the CB, as no stable states exist in between.

Initial Kinetic Testing of Fenton Reactions

To determine the rates of the various Fenton and Fenton-like reactions, UV-visible spectrophotometry was used to monitor the discoloration of a model dye in a similar method implemented under the advisement of Dr. Erick Bandala at Universidad de las Américas Puebla over the summer of 2015. To model the Fenton reaction kinetics, reactions of 100-200 mL were set up with 400 mM metal catalyst and 50 ppm Allura Red or 15 ppm N,N-dimethyl-*p*-nitrosoaniline (4NA) dye.

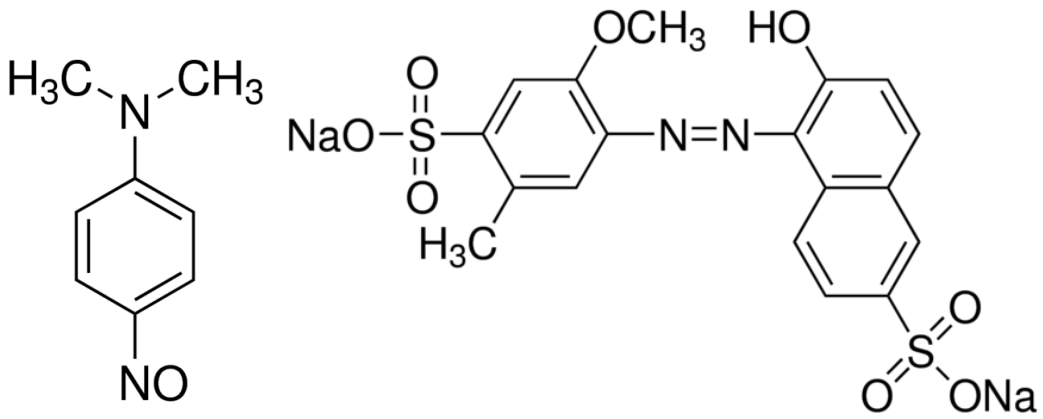

Figure 9. Allura Red and 4NA. Both structures for 4NA, a yellow dye (left), and Allura Red, a red dye (right), are provided. Both chemical structures were obtained from the Sigma-Aldrich website.

To initiate the reaction, the appropriate amount of oxidant ignoring the additive volume of the oxidant, either Oxone™ or hydrogen peroxide, was added to the reaction to equate 0.15 M concentration. The dye discoloration for Allura Red was monitored at 500 nm and 4NA at 350 nm by pouring 2-3 mL of reaction into a cuvette and returned to the reaction after the absorbance reading. The Vernier UV-visible spectrophotometer was used as it gave instant absorbance values. All absorbance readings were baselined using DI water.

To give better values for the rates of reaction, solutions with the different metals and dyes were prepared. The metal ions manganese(II), nickel(II), iron(II), and cobalt(II) were tested for reactivity with both 4NA and Allura Red using the 2401 and 2600 model Shimadzu UV-visible spectrophotometers. Kinetic traces were carried out using the same metal concentration previously used and initiated with 38.9 μL of hydrogen peroxide, maintaining 0.15 M initial oxidant concentration.

III. Results

Iron-Doped TiO_2 Testing

Iron-doped TiO_2 samples were prepared containing 0%, 1%, 2%, or 5 % iron-dopant. These were spread, dried, and sintered on ITO or FTO plates. Synthesized TiO_2 plates seemed to be darker as the amount of iron incorporated increased.

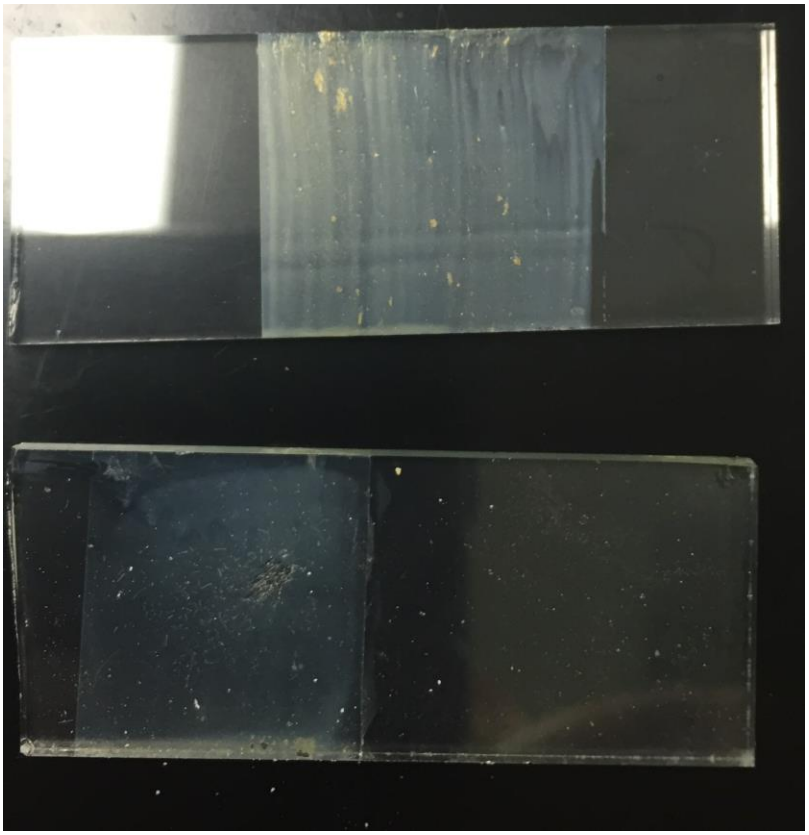

Figure 10. Synthesized TiO_2 plates. The iron-doped plates bore a visible yellow color as can be displayed by the top 2.5% plate (top) and pure TiO_2 plate (bottom). Not pictured: plates were darker with more iron and could be visibly seen between 1%, 2.5%, and 5% iron plates.

Iron-doped TiO_2 surfaces appeared flakey even after resynthesizing the catalyst and meticulous spreading. The plates of higher iron concentration were the flakiest, to the point that kinetic tests could not be performed.

In order to determine the potential of the conduction band edge, the absorbance at 780 nm was monitored while applying negative potentials to the TiO_2 plates in an anaerobic environment in order to fill the conduction band with electrons. As the concentration of iron increased, the absorbance increased (Figure 11).

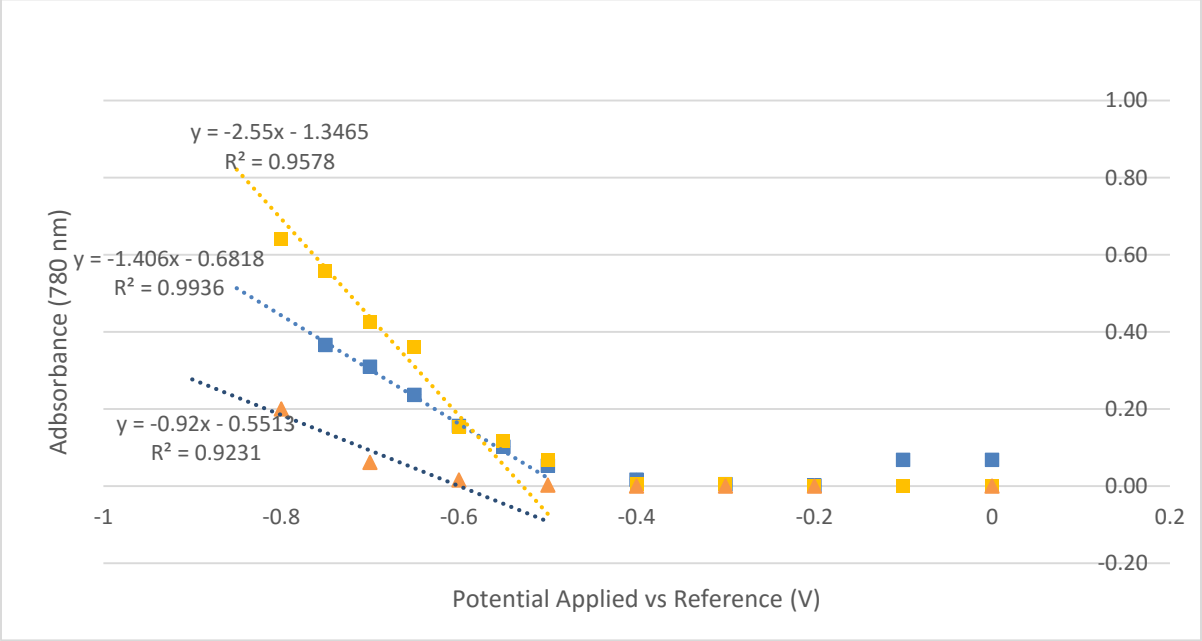

Figure 11. TiO_2 spectroelectrochemistry measuring the absorbance attributed to conduction band electrons. Each line shows the absorbance data of the TiO_2 semiconductors monitored at 780 nm while applying voltage to the FTO plate the semiconductor resided on using a platinum counter, and silver/silver chloride reference electrode in 3M KCl. The yellow squares represent 5% iron-doped TiO_2, the blue squares represent 1% iron-doped TiO_2, and the red triangles represent undoped TiO_2.

The conduction band for pure TiO_2 was found to be at -0.599V, 1% iron-doped was found at -0.485V, and 5% iron-doped was measured at -0.528V. Band gap energy was determined for four different samples of pure TiO_2.

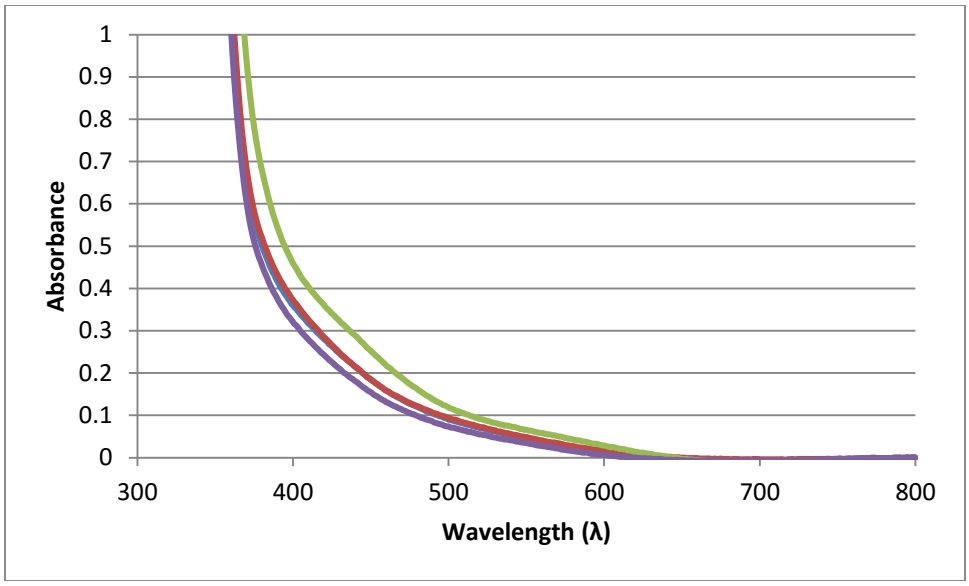

Figure 12. E_g determination for pure TiO_2. UV-visible of four different samples of solid TiO_2 on FTO plates were taken and used to determine the E_g of our samples. Linear fits were applied to the absorbance data between 345 nm – 375 nm. The x-intercepts of the lines were used to determine the band energies for the sample and an average was found to be 3.31 eV.

The same procedure was followed to determine the E_g of the 2.5% iron-doped TiO_2.

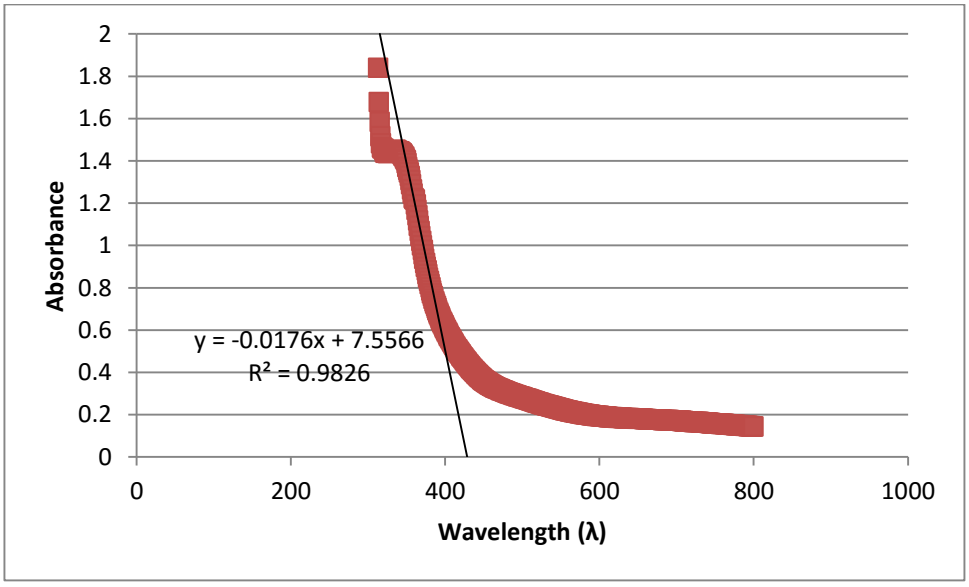

Figure 13. E_g determination for iron-doped TiO_2. UV-visible of a solid 2.5% iron-doped TiO_2 on FTO plate was taken and used to determine the E_g of the sample. A linear fit was applied to the absorbance data between 345 nm – 375 nm. The x-intercept of this line was used to determine the band energy for the sample and was found to be 2.89 eV.

Fenton Data

In order to interpret all data in molar concentrations, extinction coefficients for Allura Red at 505 nm was measured and found to be 2.1×10^4 $M^{-1}cm^{-1}$ (Figure 14).

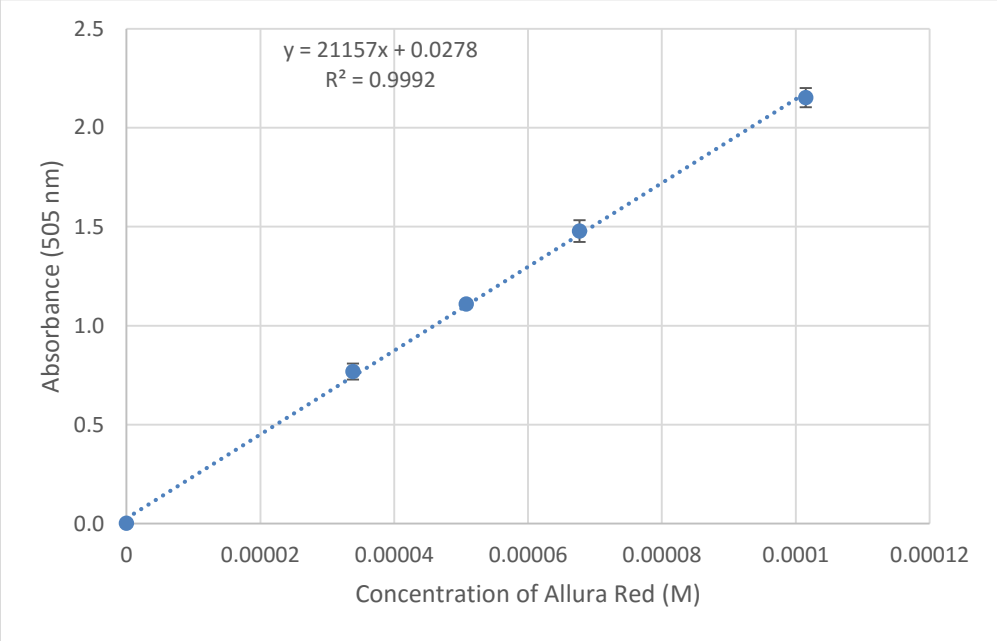

Figure 14. Extinction coefficient for Allura Red. Both trials for the determination of the extinction coefficient of Allura Red were averaged and fit with a linear line of best fit. Both trials were serial dilutions of a standard solution, prepared fresh for each trial. Error bars represent the difference in the two trials.

In order to test the Fenton reaction, dye absorbance was used a proxy for the concentration of organics in solution. Initial data were gathered to compare the catalytic activity of two metals, iron and cobalt, as well as the effectiveness of two oxidants, hydrogen peroxide and Oxone™ (Figure 15). Cobalt(II) showed no reaction with hydrogen peroxide, but showed almost complete decolorization of dye in 8 minutes using Oxone™. Ferric sulfate showed effective decolorization with Oxone™, while ferric chloride gave similar

decolorization with both Oxone™ and hydrogen peroxide. When the trials were pH controlled to pH ~2, the iron catalyzed reaction decolorized the target dye faster.

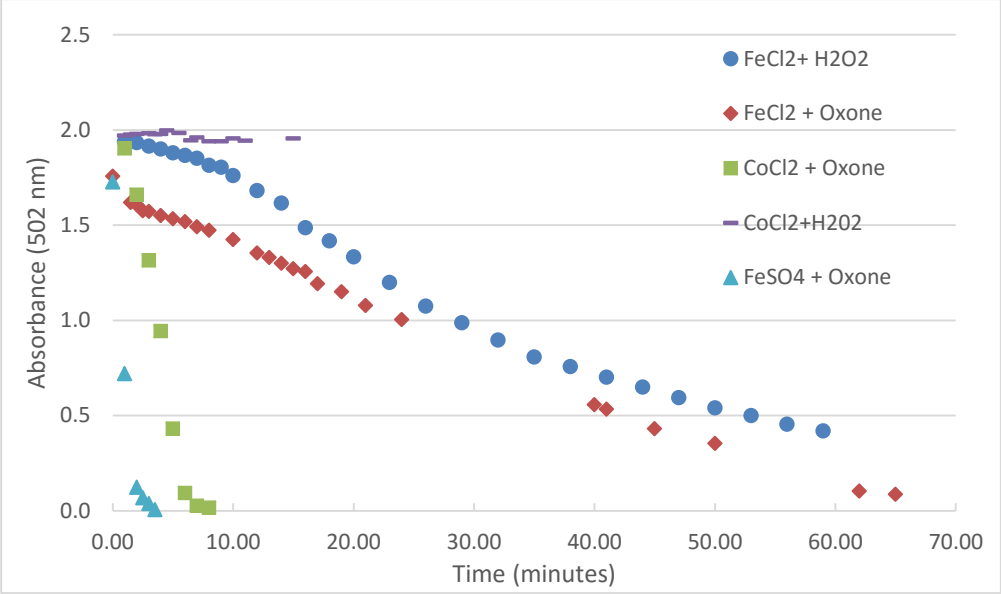

Figure 15. Initial Fenton testing. Initial testing for Fenton conditions using the LabQuest handheld UV-visible spectrophotometry setup. The purple triangles refer to testing with ferrous sulfate and Oxone™, the yellow squares refer to cobalt(II) chloride and Oxone™, red diamonds refer to ferrous chloride and Oxone™, blue circles refer to ferrous chloride and hydrogen peroxide, and the dark purple dashes refer to cobalt(II) chloride and hydrogen peroxide. The purple ferrous sulfate trial was pH controlled to around 2. Reactions were run at 200 mL volume with 50 ppm dye, 0.400 mM metal, and 0.15 M oxidant concentration. Two mL were taken from the reaction and absorbance was taken, then replaced back into the stirring reaction.

To test the effects of pH, two separate trials were run: one at pH 7 and one at pH 2. All other reaction parameters, including the concentrations of iron catalyst and H_2O_2 were kept the same between the two trials (Figure 16).

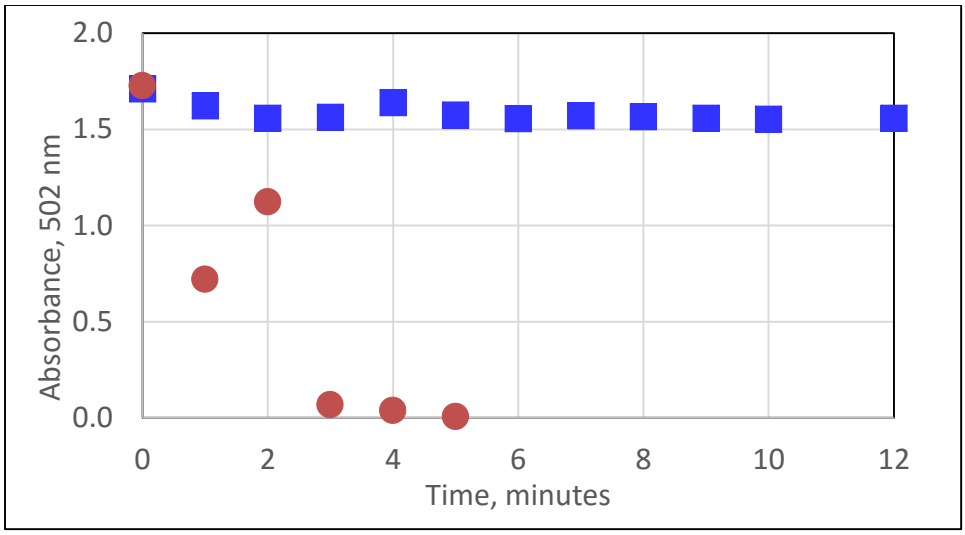

Figure 16. Fenton pH testing. Absorbance at 502 nm as a function of time for solutions containing 0.400 mM Fe(II), 0.15 M H_2O_2, 50 ppm AR at either pH 2 (red circles) or pH 7 (blue squares). Reactions were stirred and initiated by the addition of hydrogen peroxide at t=0. Aliquots of the solution (3 mL) were removed at the indicated time points and absorbance values obtained using UV-visible analysis were recorded. Trials were conducted to test the effects of pH on the decolorization of AR by the Fenton reaction.

In order to obtain more accurate time intervals, kinetics traces were obtained with the same conditions on the Shimadzu spectrophotometers (Figure 17). Metal, dye, and oxidant concentrations were kept the same and the decolorization of AR and 4NA using different metal catalysts was monitored. Reactions were initiated *in situ* by addition of hydrogen peroxide. Oxone™ could not be dissolved into concentrations that allowed for initiation of reactions without substantial dilution of the dye.

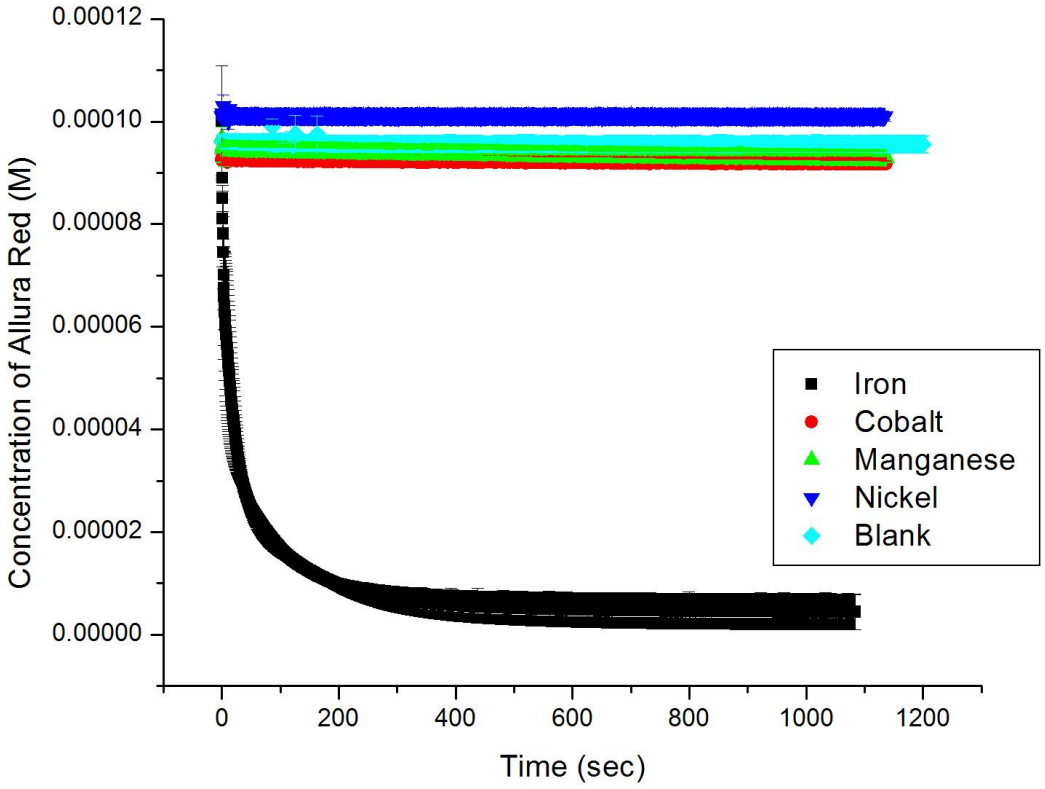

Figure 17. AR kinetic traces. Each of these lines represents a two trial average of the concentration of Allura Red after the reaction is initiated. Allura Red was monitored via UV-visible spectrophotometry at a wavelength of 500 nm. The same metal concentration of 0.401 mM and 0.15 M H_2O_2 concentration were used. Only the reaction containing iron was acidified.

Cobalt, manganese, and nickel provided no noticeable degradation of the target dye, while iron resulted in almost complete decolorization. In order to better understand the kinetics of the iron-catalyzed reaction, these data were transformed as ln[A] and 1/[A] in Figures 18 and 19, respectively. The linearity of the inverse plot suggests the reaction experiences second-order kinetics in terms of AR dye concentration.

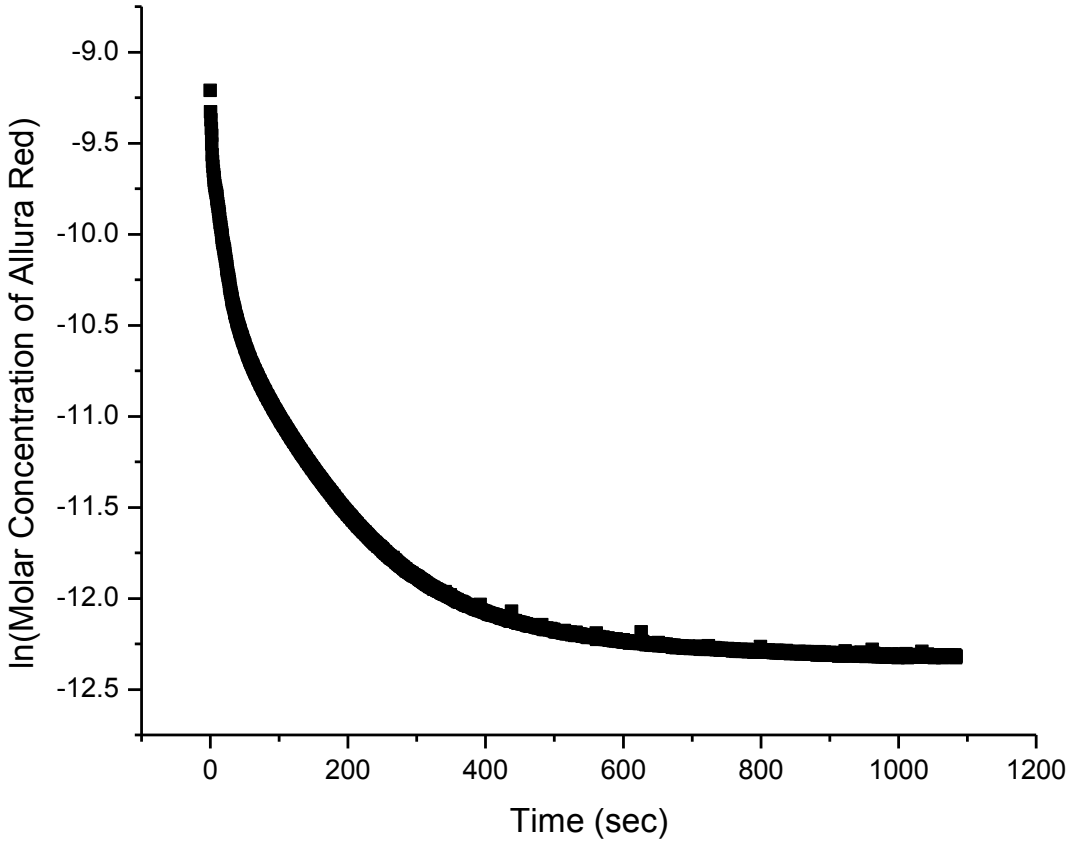

Figure 18. First-order kinetics analysis. According to first-order chemical kinetics, the natural log of the concentration of Allura Red was plotted vs. the time after reaction initiation. If this reaction were first-order in terms of dye concentration, a linear line where the slope is the rate constant would be obtained, which is not the case.

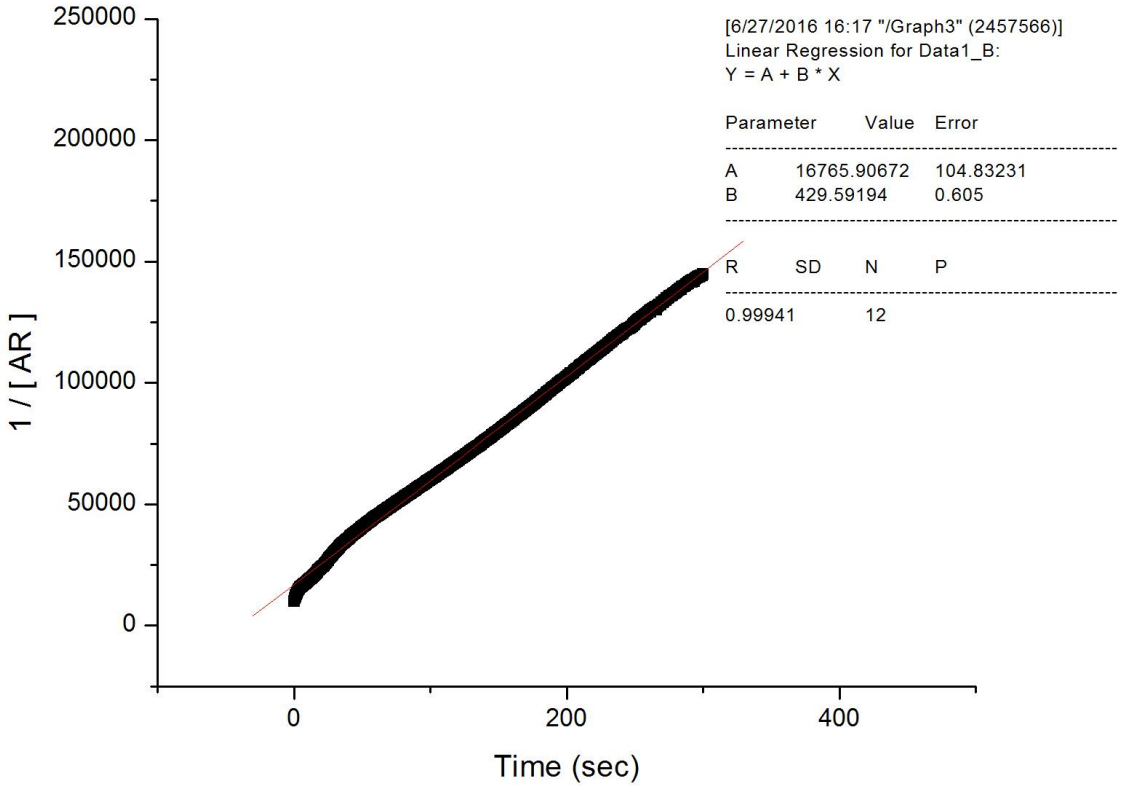

Figure 19. Second-order kinetics analysis. According to second-order chemical kinetics, the inverse of the concentration of Allura Red was plotted vs. the time after reaction initiation. When limited to the first 300 seconds of reaction, when 90% of the dye has degraded (Figure 17), the data seems to follow a pseudo-first-order fit with a rate constant of 430 $M^{-1}s^{-1}$.

The same approach was applied using 4NA as the model compound (Figure 20).

Similar decolorization rates were found compared with AR.

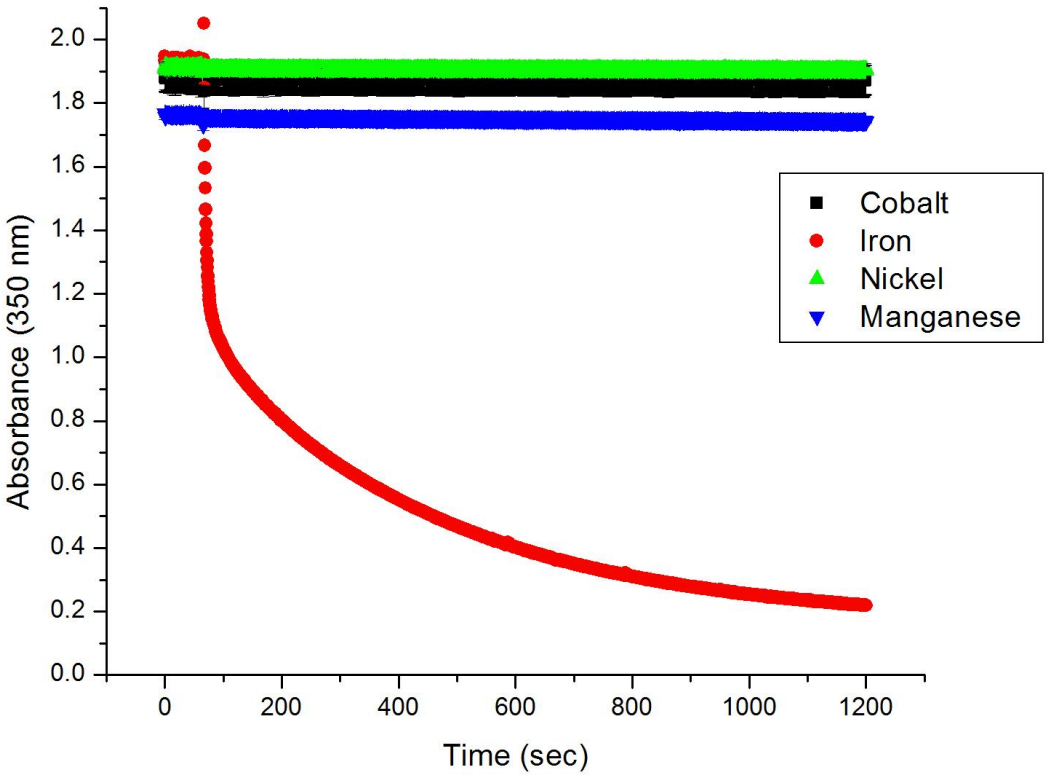

Figure 20. 4NA initial kinetic traces. Similar analysis to that previously performed with Allura Red was performed with 4NA. Metal catalyst concentrations were kept at 0.401 mM and H_2O_2 at 0.15 M. For this set of data, all reactions were acidified to pH ~2.

Similar to the AR data, only iron provided measurable dye degradation. An absorption spectrum was taken before the addition of hydrogen peroxide and after the completion of the kinetic trace to confirm the lowering of absorbance at all wavelengths and to determine if any other closely-related colored compounds were created (Figure 21).

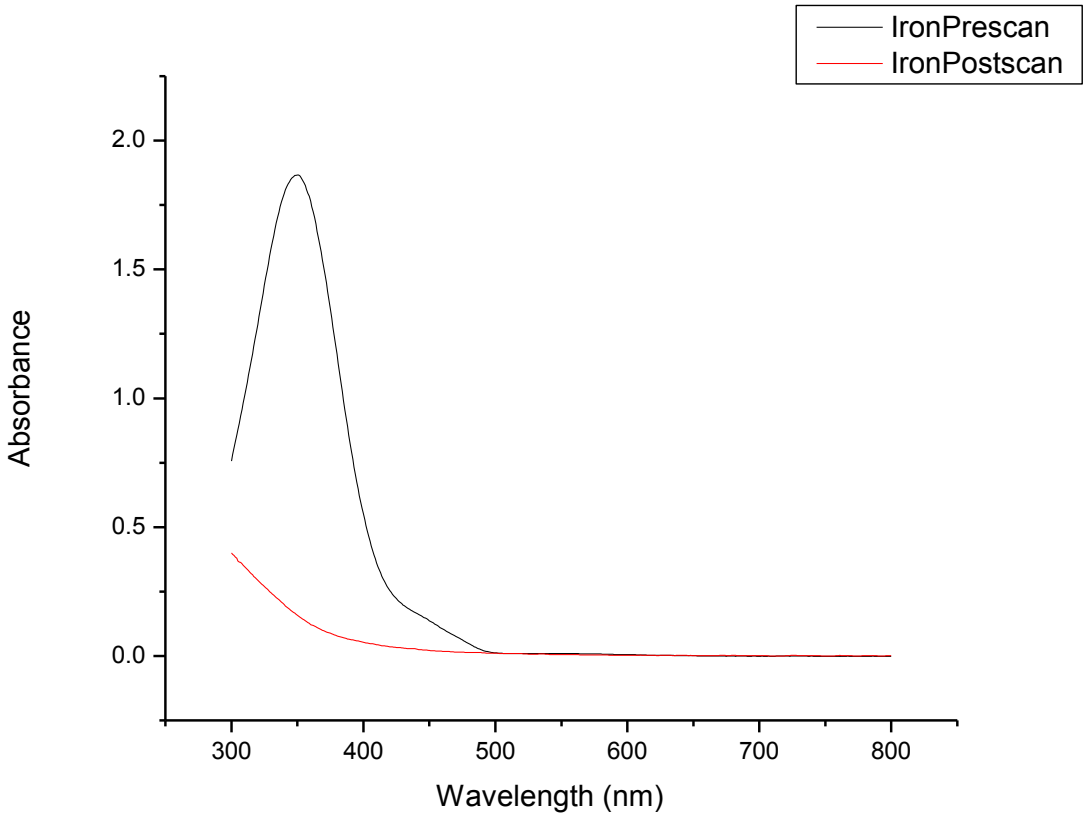

Figure 21. Absorption spectrum of 4NA degradation. The black line shows the absorbance of nondegraded 4NA dye, while the red line shows the absorbance post-Fenton reaction.

The data show a complete degradation of Allura Red and the rise in the red line is most likely due to the absorbance of any iron(III) formed. Figure 22 is reported in terms of absorbance instead of dye concentration because changing the pH changed the λ_{max} of 4NA, hinting at a pKa in the pH range of interest. This was investigated by monitoring the absorbance at 440

nm and 350 nm as a function of pH (Figure 22). This was plotted to determine the pKa.

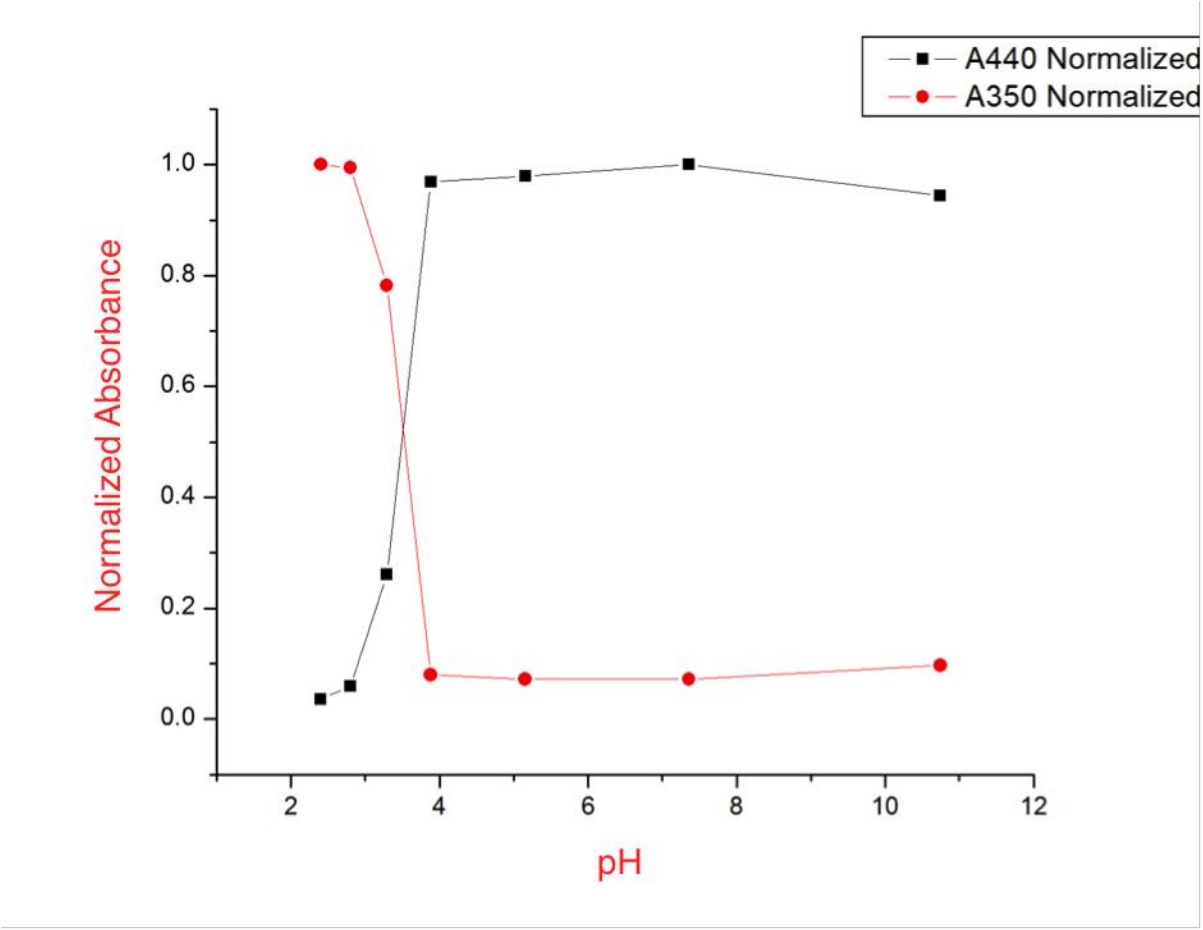

Figure 22. Normalized absorbance of 4NA. Absorbance for 4NA was monitored at 350 nm and 440 nm at varying pH. The absorbance values were normalized and plotted. The isobestic point for the different forms of 4NA was taken to be the pKa at 3.4.

The derivatives of Boltzmann exponential fits were plotted for each absorbance. The point of inflection (pKa point) turns into a maximum or minimum depending upon the trend of the data. The pKa value obtained by the intersection of the normalized absorbance data and the derivatives of the Boltzmann fits agreed. According to Figure 22, a pKa for 4NA is determined to be around 3.4, in our range of interest.

IV. Discussion

Doped TiO_2

Photocatalytic semiconductor crystals of TiO_2 with varying weight percent of iron, 1%-5%, were synthesized and spread onto FTO plates. Catalysts with the higher concentrations of iron, such as 2% or 5% (weight percent), were extremely flakey and fragile making them unusable for most testing. Synthetic methods were repeated with extreme caution, but similar results were obtained. Samples of iron-doped TiO_2 have been successfully synthesized and spread as a film by others, so the issues with our sample must be identified and corrected.[45] In order to increase the stability of iron-doped TiO_2 as a solid, better spreading methods may be implemented as physical spreading may lead to flakey, unstable solid catalyst. This may be unavoidable as incorporated iron may sufficiently destabilize the crystalline structure of the semiconductor to make it incapable of bonding to the glass. Further X-ray analysis may provide information as to whether iron is simply replacing Ti^{4+} or inducing more complicated changes in the crystalline structure. Experiments have shown that incorporating iron may result in crystalline structure modifications, such as changing the crystal structure of TiO_2 in the photocatalyst.[46]

It may also be useful to use the slurry method as opposed to immobilizing the semiconductor on an FTO plate. The slurry method involves stirring the insoluble photocatalyst in the solution and shining light on the solution. While having the TiO_2 on the FTO plate allows electrons in the conduction band of the TiO_2 to be conducted away from the solution and used to store energy, it vastly decreases the surface area of active catalyst and seems to negatively affect the performance as a photocatalyst for waste water purification. It was thought that the porous network of the semiconductor left by burning off the polymer

would increase the surface area that, along with small TiO_2 particles, would give feasible dye decolorization, but since the high surface area is tied up within the matrix and blocked in, it may still behave like a two-dimensional planar surface in terms of dye mixing.

Although further testing must be performed, very preliminary experiments showed little to no degradation. It was thought that the glass slides would block UV light and allow only visible light through. This would have given higher decolorization for iron-doped photocatalysts, but this was not seen. Flakiness of the photocatalyst or low surface area compared to the slurry method may have contributed to the poor decolorization of the photocatalyst. Iron-doped TiO_2 powders used for the slurry method have been shown to increase waste water purification over undoped photocatalyst.[46] This increase is seen using wavelengths of 300 nm to 500 nm, which may hint that iron increases the ability of the iron-doped TiO_2 powder to use sunlight as a photocatalyst. Further testing must be done on our photocatalyst to determine its ability at dye decolorization and whether immobilization on a conducting plate is the optimal utilization of it.

Incorporating increasing amounts of iron into the TiO_2 matrix lowers the conduction band as shown by Figure 11. The conduction band of pure TiO_2 was measured at -0.599 V vs Ag/AgCl, 1% iron-doped was measured at -0.485 V and 5% iron-doped was measured at -0.528 V. Our measurements show that increasing iron may shift the conduction band to a less negative potential. Measurements of the band gap of pure TiO_2 and 2.5% iron-doped TiO_2 strengthen the argument that iron incorporation is affecting the photocatalytic properties of the semiconductor. The band gap of pure TiO_2 was experimentally determined to be 3.31 eV, slightly higher than the literature value of 3.2 eV.[32] The value for 2.5% iron-doped TiO_2

was lower at 2.89 eV. This agrees with the literature, which have shown increased amounts of iron shift the band gap of TiO_2 towards absorbing visible light.[45,47]

More complete analysis of samples must be conducted in order to determine how the dopant is shifting the energetics of the semiconductor. The dopant can have three effects on the semiconductor. It can lower the energy of the CB, raise the energy of the VB, or introduce a mid-band gap state capable of gaining or losing electrons (Figure 23).

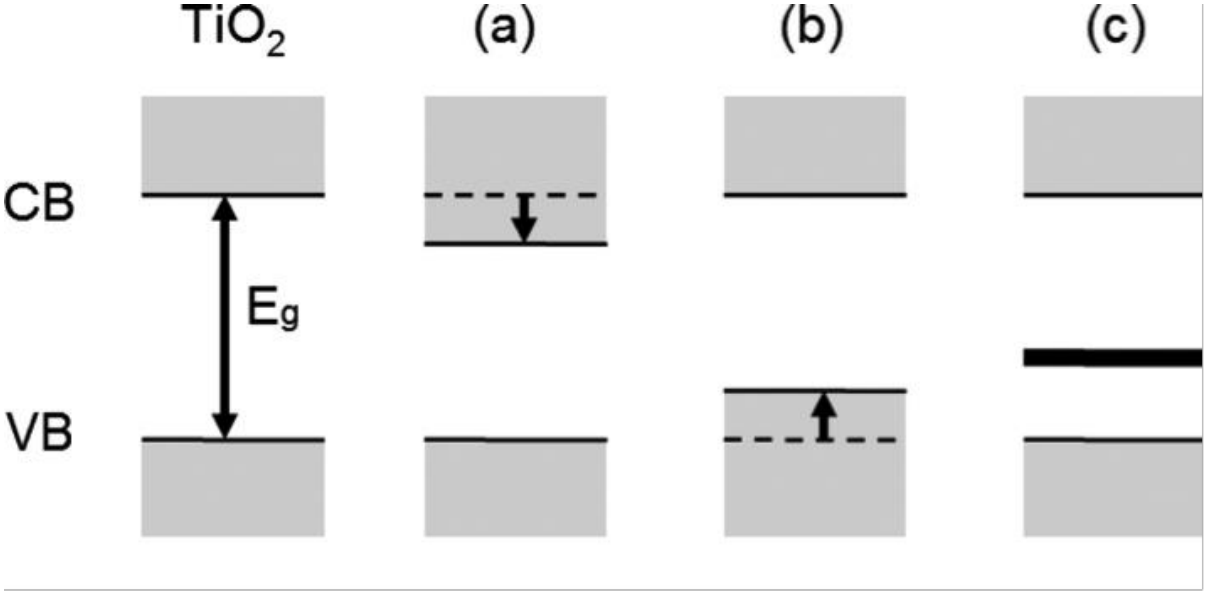

Figure 23. Possible dopant effects. Dopants can have three possible effects on the semiconductor. The dopant can lower the energy of the CB (a), raise the energy of the VB (b), or introduce a mid-band gap state (c).

Complete data for each dopant concentration was not obtained, but the conduction band shifted 0.071 V for the 1% iron-doped and 0.114 V for the 5% iron-doped samples. Based upon these values, the 0.42 V shift in the band gap energy cannot be fully explained by the shift in the conduction band. This would hint that incorporating iron into the TiO_2 shifts both the conduction band and valence band, a combination of (a) and (b) in Figure 23.

While the spectroscopic method derived from Redmond *et al.* for band gap determination has been used for years, it does not account for the temperature dependence of the conductance band energy.[44] A method developed by Ondersma and Hamann accounts for

this relationship and provides a more accurate value for the conductance band energy. [47] This method may be implemented in order to provide more accurate values for the band gap energy and to verify the values obtained experimentally.

Further testing must be done to determine the amount of iron actually incorporate into the catalyst. This would include energy-dispersive X-ray spectroscopy. Testing the catalytic activity of the catalysts must also be done to determine if the catalyst deposited on the surface has practical use.

Fenton Chemistry

Data similar to Figure 15 were collected in Mexico using PMS instead of AR. Initial data collected in Dr. Bandala's laboratory hinted that the Co^{2+}/PMS, Fenton-like system may outperform the standard Fe^{2+}/H_2O_2 Fenton reaction. Upon reproducing the experiment, it was found that adjusting the pH altered the decolorization of the iron catalyst. This is due to the solubility properties of iron(III) in aqueous solutions. This means that data collected in Dr. Bandala's laboratory may not have looked at the complete picture, as it does not take into account the need to adjust pH for the ferrous iron system to prevent the iron catalyst from precipitating from solution. A more accurate comparison would be between the iron and cobalt PMS systems, which proved to be similar as shown in Figure 15.

It was found that iron was the only metal tested capable of decolorization via the degradation of H_2O_2. It was assumed that this reaction would follow first-order kinetics in terms of the dye, as the metal catalyst and oxidant concentration seemed to be significantly higher. This assumption was proved wrong, and a second-order kinetic fit was applied. This resulted in a linear fit with a pseudo-second-order rate constant of 430 $M^{-1}s^{-1}$. This could mean that the reaction is dependent upon two dye molecules colliding in solution. Further

analysis is needed in order to determine rates and order of the Fenton reaction in terms of other reagents. In this situation, metal and oxidant concentrations were high, but other experiments could be set up to determine the order of each reactant on the overall kinetic order of the reaction.

Hambourger's lab chose to use Allura Red as a model dye, but Dr. Bandala had chosen to work with the 4NA. Dr. Bandala cited a documented history of 4NA in use as a radical scavenger and to spin trap ROS and radicals for identification.[48] The ability of these two dyes to react with radical species could be different, generating misleading data for either of the dyes. Upon attempting to compare, it was noticed that lowering the pH of a given trial would decreased the intensity of the color. Through experimentation it was discovered that 4NA has a pKa around 3.4, which shifts its absorption profile. This shift in absorbance may skew data collected at one wavelength and makes data collected with 4NA suspect. Protonation of the dimethylamine group is probably happening, as the anilinium ion has a pKa of 4.63, while nitrosoaniline is not readily protonated. Data collected may show conversion between different protonation states of 4NA and may not reflect actual degradation.

Decolorization of dyes is used as a means to estimate complete organic degradation. While absorbance is easy to monitor, it provides no information on mineralization or the intermediate compounds formed during degradation. Methods such as TOC and COD provide better information regarding mineralization, but are difficult to monitor, especially in real-time.

VI. Future Work

Both the Fenton reaction, its derivatives, and TiO_2 have promise in waste water purification. While both of these methods of waste water purification fall under the umbrella of AOP, one involves an external oxidant and the other a semiconductor. It seems that the Fenton reaction is capable of producing hydroxyl radicals capable of oxidation at a much higher rate than TiO_2, but the pros and cons of each method should be analyzed. A semiconductor that does not require an external oxidant or removal after purification has considerable benefits over the Fenton reaction. One method should be chosen for investigation and focused upon for waste water purification.

In order to further understand the iron-doped TiO_2 system, Ondersma's method for conductance and valence band determination should be investigated and implemented.[47] Alternative methods for spreading synthesized catalyst should also be explored in order to fix the flaking plate problem. Catalytic testing must also be performed to determine the dye decolorization capabilities of the semiconductors. Scanning electron microscope images of the catalyst surface may also provide evidence that iron has been incorporated into the matrix of the catalyst. Elemental analysis of these images using energy-dispersive X-ray spectroscopy should also be performed.

To advance the project on Fenton chemistry, specific metals should be chosen and investigated for reactivity with PMS. Additional access to total organic carbon and chemical oxygen demand analyzers may help to determine which Fenton-like reaction derivative would prove most effective for removing recalcitrant pollutants. Analysis of organic degradation products via IR, HPLC, and NMR may provide further information on

breakdown pathways and give further information on these methods for waste water purification.

VI. Conclusions

While recalcitrant pollutants and ECs remain a huge problem to our society, a simple fix has yet to be found. Further work must be done to determine the effectiveness of iron-doped TiO_2 for waste water purification. Our initial results show both the conduction band shifting to less negative potentials and the band gap narrowing as iron is incorporated into the semiconductor. Further testing must be done to determine the optimum iron concentration for photocatalytic activity in sunlight. Fenton chemistry seems to be a better solution for waste water purification even though the exact mechanism of the reaction is still unknown. The Fe^{2+}/H_2O_2 and Co^{2+}/PMS Fenton systems seem to have similar decolorization rates, while Co^{2+}/PMS seems to outperform the Fe^{2+}/PMS. Although promising, Fenton-like derivatives, including using Oxone™ as an oxidant or replacing the metal catalyst, do not seem to provide any increased decolorization of Allura Red when compared to the normal system.

References

1. *Progress on sanitation and drinking water*; World Heath Organization: New York, **2015**.
2. Mekonnen, M. M.; Hoekstra, A. Y., Four billion people facing severe water scarcity. *Science Advances* **2016,** *2* (2).
3. Bouabid, A.; Louis, G. E., Capacity factor analysis for evaluating water and sanitation infrastructure choices for developing communities. *Journal of Environmental Management* **2015,** *161*, 335-343.
4. Barnes, K. K.; Kolpin, D. W.; Furlong, E. T.; Zaugg, S. D.; Meyer, M. T.; Barber, L. B., A national reconnaissance of pharmaceuticals and other organic wastewater contaminants in the United States — I) Groundwater. *Science of the Total Environment* **2008,** *402* (2–3), 192-200.
5. Sornalingam, K.; McDonagh, A.; Zhou, J. L., Photodegradation of estrogenic endocrine disrupting steroidal hormones in aqueous systems: Progress and future challenges. *Science of the Total Environment* **2016,** *550*, 209-224.
6. Schmidt, T. C.; Field, J., Water analysis for emerging chemical contaminants. *Analytical Chemistry* **2016,** *88* (3), 1495.
7. Alistair, B. A. B., The environmental side effects of medication. In *EMBO Reports*, **2004**; Vol. 5, 1110-1116.
8. Kuperman, R. G.; Checkai, R. T.; Simini, M.; Phillips, C. T.; Kolakowski, J. E.; Kurnas, C. W., Weathering and aging of 2,4,6-trinitrotoluene in soil increases toxicity to potworm *Enchytraeus crypticus*. *Environmental Toxicology and Chemistry* **2005,** *24* (10), 2509-2518.
9. Orton, F.; Tyler, C. R., Do hormone-modulating chemicals impact on reproduction and development of wild amphibians? *Biological Reviews* **2015,** *90* (4), 1100-1117.
10. Kendall, R., Wildlife toxicology: where we have been and where we are going. *Journal of Environmental Analytical Toxicology* **2016,** *6* (1).
11. Grady Jr, C. L.; Daigger, G. T.; Love, N. G.; Filipe, C. D., *Biological Wastewater Treatment*. CRC press: **2011**.
12. Wick, A.; Fink, G.; Joss, A.; Siegrist, H.; Ternes, T. A., Fate of beta-blockers and psycho-active drugs in conventional wastewater treatment. *Water Research* **2009,** *43* (4), 1060-1074.
13. Malato, S.; Fernandez-Ibanez, P.; Maldonado, M. I.; Blanco, J.; Gernjak, W., Decontamination and disinfection of water by solar photocatalysis: Recent overview and trends. *Catalysis Today* **2009,** *147*, 1-59.
14. Apel, K.; Hirt, H., Reactive oxygen species: metabolism, oxidative stress, and signal transduction. *Annual Review of Plant Biology* **2004,** *55* (1), 373-399.
15. Fenton, H. J. H., LXXIII.-Oxidation of tartaric acid in presence of iron. *Journal of the Chemical Society, Transactions* **1894,** *65*, 899-910.
16. Fenton, H. J. H.; Jackson, H. J., I.—The oxidation of polyhydric alcohols in presence of iron. *Journal of the Chemical Society, Transactions* **1899,** *75*, 1-11.
17. Fenton, H. J. H.; Jones, H., VII.—The oxidation of organic acids in presence of ferrous iron. Part I. *Journal of the Chemical Society, Transactions* **1900,** *77*, 69-76.

18. Halliwell, B., Reactive oxygen species in living systems: Source, biochemistry, and role in human disease. *The American Journal of Medicine* **1991,** *91* (3, Supplement 3), S14-S22.
19. Circu, M. L.; Aw, T. Y., Reactive oxygen species, cellular redox systems, and apoptosis. *Free Radical Biology and Medicine* **2010,** *48* (6), 749-762.
20. Strlic, M.; Kolar, J.; Pihlar, B., The effect of metal ion, pH and temperature on the yield of oxidising species in a Fenton-like system determined by aromatic hydroxylation. *Acta Chimica Slovenica* **1999,** *46* (4), 555-566.
21. Barbusinski, K., Fenton reaction - controversy concerning the chemistry. *Ecological Chemistry and Engineering* **2009,** *16* (3), 347.
22. Yamamoto, N.; Koga, N.; Nagaoka, M., Ferryl–oxo species produced from Fenton's reagent via a two-step pathway: minimum free-energy path analysis. *The Journal of Physical Chemistry B* **2012,** *116* (48), 14178-14182.
23. Goldstein, S.; Meyerstein, D.; Czapski, G., The Fenton reagents. *Free Radical Biology and Medicine* **1993,** *15* (4), 435-445.
24. Neamtu, M.; Yediler, A.; Siminiceanu, I.; Kettrup, A., Oxidation of commercial reactive azo dye aqueous solutions by the Photo-Fenton and Fenton-like processes. *Journal of Photochemistry and Photobiology A: Chemistry* **2003,** *161* (1), 87-93.
25. Kuan, C.-C.; Chang, S.-Y.; Schroeder, S. L. M., Fenton-like oxidation of 4-chlorophenol: homogeneous or heterogeneous? *Industrial & Engineering Chemistry Research* **2015,** *54* (33), 8122-8129.
26. (a) Beverskog, B.; Puigdomenech, I., Revised Pourbaix diagrams for iron at 25–300 °C. *Corrosion Science* **1996,** *38* (12), 2121-2135.
(b) Delahay, P.; Pourbaix, M.; Van Rysselberghe, P., Potential-pH diagrams. *Journal of Chemical Education* **1950,** *27* (12), 683.
27. Blanco, M.; Martinez, A.; Marcaise, A.; Aranzabe, E.; Aranzabe, A., Heterogeneous Fenton catalyst for the efficient removal of azo dyes in water. *American Journal of Analytical Chemistry* **2014,** *5*, 490-499.
28. Ramirez, J. H.; Costa, C. A.; Madeira, L. M.; Mata, G.; Vicente, M. A.; Rojas-Cervantes, M. L.; López-Peinado, A. J.; Martín-Aranda, R. M., Fenton-like oxidation of Orange II solutions using heterogeneous catalysts based on saponite clay. *Applied Catalysis B: Environmental* **2007,** *71* (1–2), 44-56.
29. Fernandez, J.; Maruthamuthu, P.; Renken, A.; Kiwi, J., Bleaching and photobleaching of Orange II within seconds by the oxone/Co^{2+} reagent in Fenton-like processes. *Applied Catalysis B: Environmental* **2004,** *49* (3), 207-215.
30. Kim, J.; Edwards, J. O., A study of cobalt catalysis and copper modification in the coupled decompositions of hydrogen peroxide and peroxymonosulfate ion. *Inorganica Chimica Acta* **1995,** *235* (1), 9-13.
31. Lutz, J.; Schlangenotto, H.; Scheuermann, U.; Doncker, R., Semiconductor properties. *Semiconductor Power Devices: Physics, Characteristics, Reliability*, Springer Berlin Heidelberg: Berlin, Heidelberg, **2011**; 17-75.
32. Linsebigler, A. L.; Lu, G.; Yates Jr, J. T., Photocatalysis on TiO_2 surfaces: principles, mechanisms, and selected results. *Chemical Reviews* **1995,** *95* (3), 735-758.
33. Khataee, A. R.; Pons, M. N.; Zahraa, O., Photocatalytic decolorisation and mineralisation of orange dyes on immobilised titanium dioxide nanoparticles. *Water Science and Technology* **2010,** *62* (5), 1112-1120.

34. Dvoranova, D.; Barbeirikova, Z.; Brezova, V., Radical intermediates in photoinduced reactions on TiO_2. *Molecules* **2014,** *19*, 17279.
35. Fujishima, A.; Rao, T. N.; Tryk, D. A., Titanium dioxide photocatalysis. *Journal of Photochemistry and Photobiology C: Photochemistry Reviews* **2000,** *1* (1), 1-21.
36. Biernat, K.; Malinowski, A.; Gnat, M., *The possibility of future biofuels production using waste carbon dioxide and solar energy*. **2013**.
37. Răileanu, M.; Crişan, M.; Niţoi, I.; Ianculescu, A.; Oancea, P.; Crişan, D.; Todan, L., TiO_2-based nanomaterials with photocatalytic properties for the advanced degradation of xenobiotic compounds from water. a literature survey. *Water, Air, & Soil Pollution* **2013,** *224* (6), 1-45.
38. Dana Desonie, P. D. Solar Energy on Earth. http://www.ck12.org/earth-science/Solar-Energy-on-Earth/lesson/Solar-Energy-on-Earth-HS-ES/.
39. Wang, X. H.; Li, J. G.; Kamiyama, H.; Moriyoshi, Y.; Ishigaki, T., Wavelength-sensitive photocatalytic degradation of methyl orange in aqueous suspension over iron(III)-doped TiO_2 nanopowders under UV and visible light irradiation. *The Journal of Physical Chemistry B* **2006,** *110* (13), 6804-6809.
40. Reisner, E.; Powell, D. J.; Cavazza, C.; Fontecilla-Camps, J. C.; Armstrong, F. A., Visible light-driven H_2 production by hydrogenases attached to dye-sensitized TiO_2 nanoparticles. *Journal of the American Chemical Society* **2009,** *131* (51), 18457-18466.
41. Oliveros, E.; Legrini, O.; Hohl, M.; Müller, T.; Braun, A. M., Industrial waste water treatment: large scale development of a light-enhanced Fenton reaction. *Chemical Engineering and Processing: Process Intensification* **1997,** *36* (5), 397-405.
42. Savage, N.; Diallo, M. S., Nanomaterials and water purification: opportunities and challenges. *Journal of Nanoparticle research* **2005,** *7* (4-5), 331-342.
43. Kang, M. G.; Park, N.-G.; Park, Y. J.; Ryu, K. S.; Chang, S. H., Manufacturing method for transparent electric windows using dye-sensitized TiO_2 solar cells. *Solar Energy Materials & Solar Cells* **2003,** *75*, 475-479.
44. Redmond, G.; Fitzmaurice, D., Spectroscopic determination of flatband potentials for polycrystalline TiO_2 electrodes in nonaqueous solvents. *Journal of Physical Chemistry* **1993,** *97* (7), 1426-1430.
45. Sonawane, R. S.; Kale, B. B.; Dongare, M. K., Preparation and photo-catalytic activity of Fe TiO_2 thin films prepared by sol–gel dip coating. *Materials Chemistry and Physics* **2004,** *85* (1), 52-57.
46. Crişan, M.; Răileanu, M.; Drăgan, N.; Crişan, D.; Ianculescu, A.; Niţoi, I.; Oancea, P.; Şomăcescu, S.; Stănică, N.; Vasile, B.; Stan, C., Sol–gel iron-doped TiO_2 nanopowders with photocatalytic activity. *Applied Catalysis A: General* **2015,** *504*, 130-142.
47. Hamann, J. W. O. T. W., Conduction band energy determination by variable temperature spectroelectrochemistry. *Energy Environmental Science* **2012,** *5*, 9476-9480.
48. Kraljić, I.; Mohsni, S. E., A new method for the detection of singlet oxygen in aqueous solutions. *Photochemistry and Photobiology* **1978,** *28* (4-5), 577-581.